

Chapter 6 The stratigraphy and sedimentology of the Pleistocene minerogenic sediments of the Gordano Valley

6.1 Introduction

This chapter addresses the second objective: to establish the stratigraphy and ages of the Pleistocene sedimentary units. The stratigraphy and sedimentology of seven percussion cores extracted for minerogenic sediment analysis is presented using the methods outlined in Chapter 4 (sections 4.7, 4.8, 4.9, 4.10 and 4.11). The stratigraphy of each core is described first, followed by results from analysis of sediment particle size, gravel clast lithology, surface features and morphology, geochemistry, palaeontology and geochronology.

6.2 Stratigraphy

The locations of the percussion cores taken for stratigraphical analysis and age determination are shown in Figure 4.11; field details and locations are given in Table 6.1. A key to the symbols used in the stratigraphic descriptions is provided on p 85.

The upper metre of core PG (2.55 to 1.55 m OD) was recovered in the core liner which then became wedged in the corer and proved impossible to remove in the field. It was therefore brought back to the laboratory for extraction. Subsequent coring was carried out using an open face corer. This allowed sediment to be recovered to 0.43 m OD, but the core section had to be returned intact to the laboratory for logging and processing. Because these difficulties resulted in some disturbance of sediment and unclear lower boundaries, a second borehole, PGA, was sunk adjacent to this. However, there were also difficulties with the extraction of the liner from this core, particularly with the middle section, resulting in a highly disturbed section of core.

There were also difficulties with the extraction of the liner from cores CGA and CGB, but the resulting disturbance to the sediments was less severe than for cores PG and PGA. For cores NR, CM and TG the material became very dense with increased depth below the surface and recovery of further samples was not possible with the equipment used. The stratigraphy of core TG is secure between 2.08 and -1.27 m OD but subsequent

over-sampling resulted in the loss of some material between -1.27 and -2.27 m OD. It is estimated that approximately 40 cm of material was lost, but this material appeared to be of the same nature as that recovered at the base of the previous core section at -1.27 m OD.

Table 6.1: Field details of percussion cores

Core	Site	GPS co-ordinates	Surface altitude m (OD)	Peat thickness (m)	Minerogenic surface altitude m (OD)	Thickness of minerogenic sediments recovered (m)
PG	Weston Moor	N 51° 27.654' W 002° 47.934'	5.054	2.50	2.554	2.12
PGA	Weston Moor	N 51° 27.654' W 002° 47.934'	5.054	2.54	2.514	2.46
CGA	Weston Moor	N 51° 27.680' W 002° 48.060'	5.180	2.00	3.180	1.83
CGB	Weston Moor	N 51° 27.690' W 002° 48.103'	5.143	2.10	3.043	1.89
NR	Weston Moor	N 51° 27.308' W 002° 47.859'	5.125	2.45	2.675	3.35
CM	Clapton Moor	N 51° 27.618' W 002° 47.575'	5.345	2.35	2.995	2.65
TG	Weston Moor	N 51° 27.504' W 002° 48.055'	5.070	2.99	2.080	4.75

As a consequence of the difficulties experienced extracting core liners, some basal contacts are unclear and in some cases the stratigraphic description has been pieced together from the information available. The effects on stratigraphy are discussed in individual core sub-sections. Full stratigraphic descriptions are provided in Appendix II.

6.2.1 Stratigraphy of core PG

The stratigraphic log of core PG is illustrated in Figure 6.1.

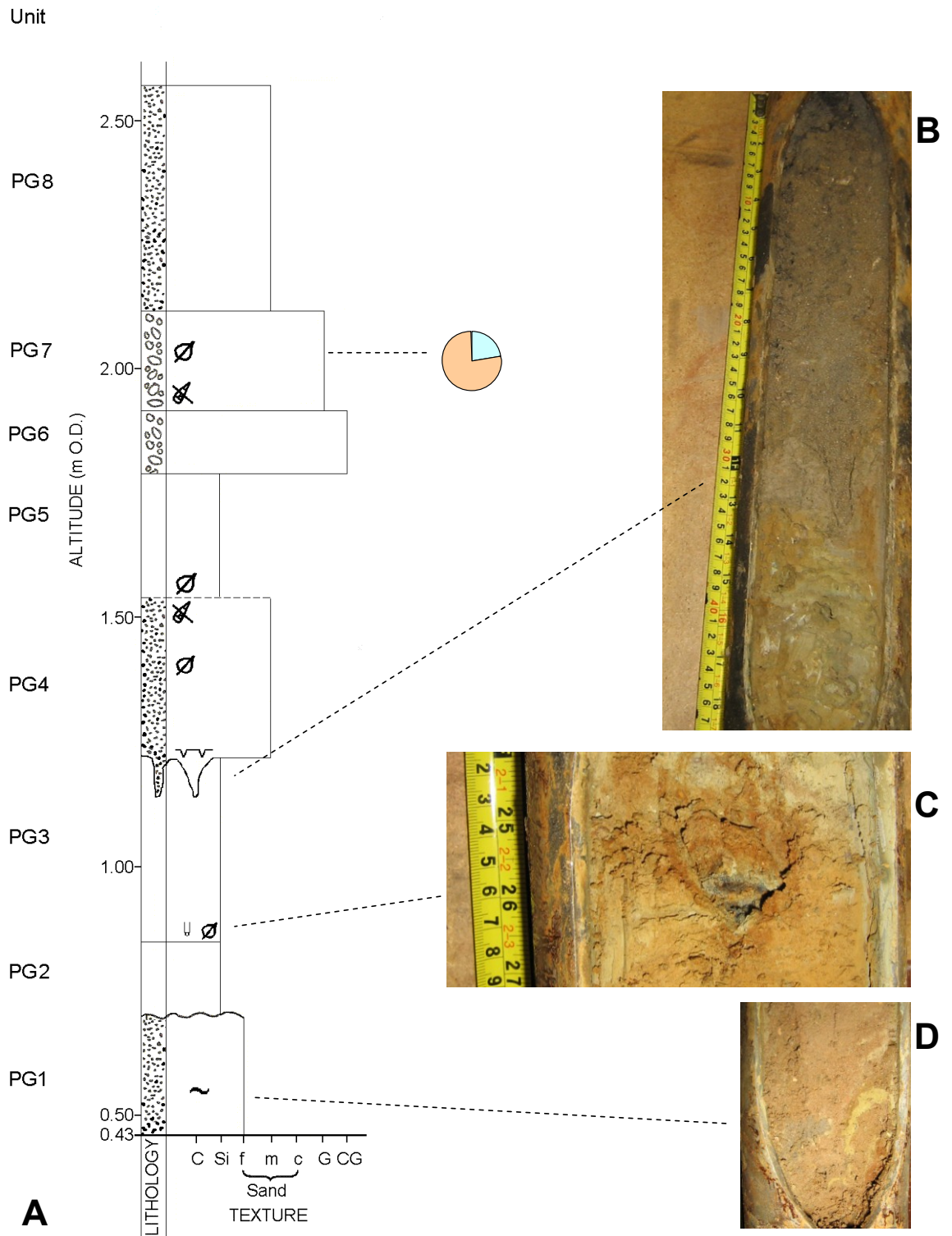


Figure 6.1: A. Stratigraphy of core PG; stratigraphic units are shown on the left. B. Sand filled crack at boundary between PG4 and PG3. C. Wood fragment (arrowed) and associated orange mottling in PG3. D. Silt folded into fine sand in PG1

Boundaries between units, with the exception of the unclear lower boundaries of PG5 and PG6, are sharp, and most are also planar, suggesting separate depositional events separated by periods of erosion or non-deposition (Tucker 2003). However, the boundary between PG3 and PG4 (Figure 6.1B) is irregular and shows a vertical wedge which is infilled with sand. The infill is the same material as PG4 except at the very base of the wedge, where there is a very thin infill of greenish grey (Gley 1 5/1 10Y) silt. The wedge measures 1.6 cm across the top, narrowing to 1 cm at the base, and is 7.3 cm in length. Towards the base of PG1 a 2 cm silt inclusion is folded into the fine sand (Figure 6.1D).

6.2.2 Stratigraphy of core PGA

The stratigraphic log of core PGA is illustrated in Figure 6.2. All identifiable boundaries in core PGA are sharp; eight are sharp and planar and five are sharp and irregular. The boundaries between PGA6 and PGA7 and between PGA11 and PGA12 are irregular and dipping and the upper boundary of PGA4 and PGA5 is irregular and convex-up. The central core section, containing units PGA7 to PGA14, was recovered piecemeal with both the upper and lower parts being removed separately in extraction of the liner. The stratigraphic description has therefore been pieced together from the information available and as a consequence four basal contacts are unclear. Some sand was lost from the upper part of the section, and part of the core (a silt unit) stretched to fill the space left so that the total thickness of this unit had to be calculated from the total section thickness. The missing upper part of this section measured 36 cm; however, the recovered material measured 69 cm, indicating that it had undergone some stretching. The missing lower part measured 16 cm; the remaining central portion measured 44 cm. In the lowest core section, containing units PGA1 to PGA7, the uppermost 10 cm was also disturbed, but appeared to be a continuation of both the preceding and following deposits.

A cluster of white granules was found in PGA17, approximate diameter of individual granules was 2 mm. Soft white oval-shaped carbonate nodules with a slightly irregular outline were found in PGA5 (Figure 6.2D), becoming increasingly numerous towards the base. The long axis of these nodules measured 0.5-1 cm.

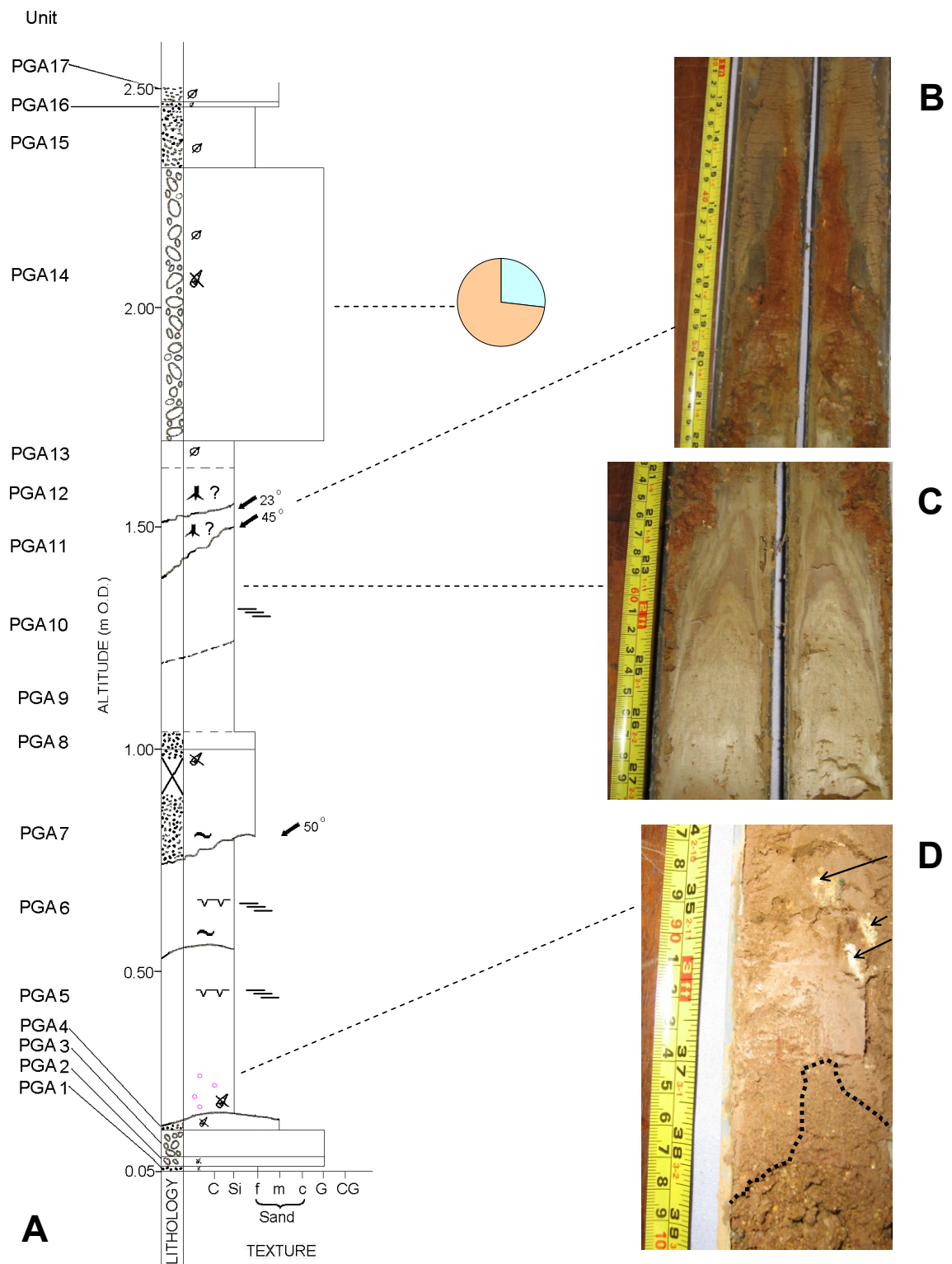


Figure 6.2: A. Stratigraphy of core PGA; stratigraphic units are shown on the left. B. Root trace in PGA11. C. Liesegang rings in PGA10. Root trace of PGA11 is visible at the top of the picture. D. Carbonate nodules (arrowed) in PGA5. Dotted line marks transition from PGA5 (reddish brown silt) to PGA4 (yellowish red sand)

PGA10 displays Liesegang rings (Figure 6.2C); their contorted, convex appearance is probably coring induced (Evans & Benn 2004). Other possible signs of core disturbance include: stretching of sediments as a result of core liner extraction problems, probably responsible for the many fine cracks recorded in the silt units PGA5, PGA6 and PGA10; a sand inclusion in silt unit PGA6, apparently of similar colour and texture to PGA7, has been folded into PGA6; a silt inclusion in sand unit PGA7 which could be from PGA8 or PGA6, although its light yellowish brown colour suggests it is from PGA6.

6.2.3 Stratigraphy of core CGA

The stratigraphic log of core CGA is illustrated in Figure 6.3. A number of the boundaries in CGA are gradational, often in sequence, and preceded or succeeded by sharp basal contacts. CGA2, CGA3, CGA4, CGA9 and CGA13 have sharp planar basal contacts; other sharp contacts are irregular. The changes in CGA4, CGA5 and CGA6 show similarities to a soil profile, with gradual changes between units and increasingly darker colour with increasing altitude (Figure 6.3C), whilst CGA11 displays a root trace. Blackened concretions of pebbles are present in CGA6 and many of the units demonstrate iron mottling (Figure 6.3B). The fine rippled laminations in CGA2 (Figure 6.3D) probably indicate deposition in the presence of flowing water.

6.2.4 Stratigraphy of core CGB

The stratigraphic log of core CGB is illustrated in Figure 6.4. With one exception, the contact between CGB2 and CGB3 which is gradational and indicates continuous deposition, the boundaries between units in CGB are sharp suggesting discrete depositional events separated by periods of erosion or non-deposition (Tucker 2003). Sharp boundaries with overlying coarse sediment between CGB6 and CGB7, CGB8 and CGB9 and CGB12 and CGB13 indicate an erosional surface (Tucker 2003) whilst the boundary between CGB3 and CGB4 is unconformable and probably represents a long interval of non-deposition.

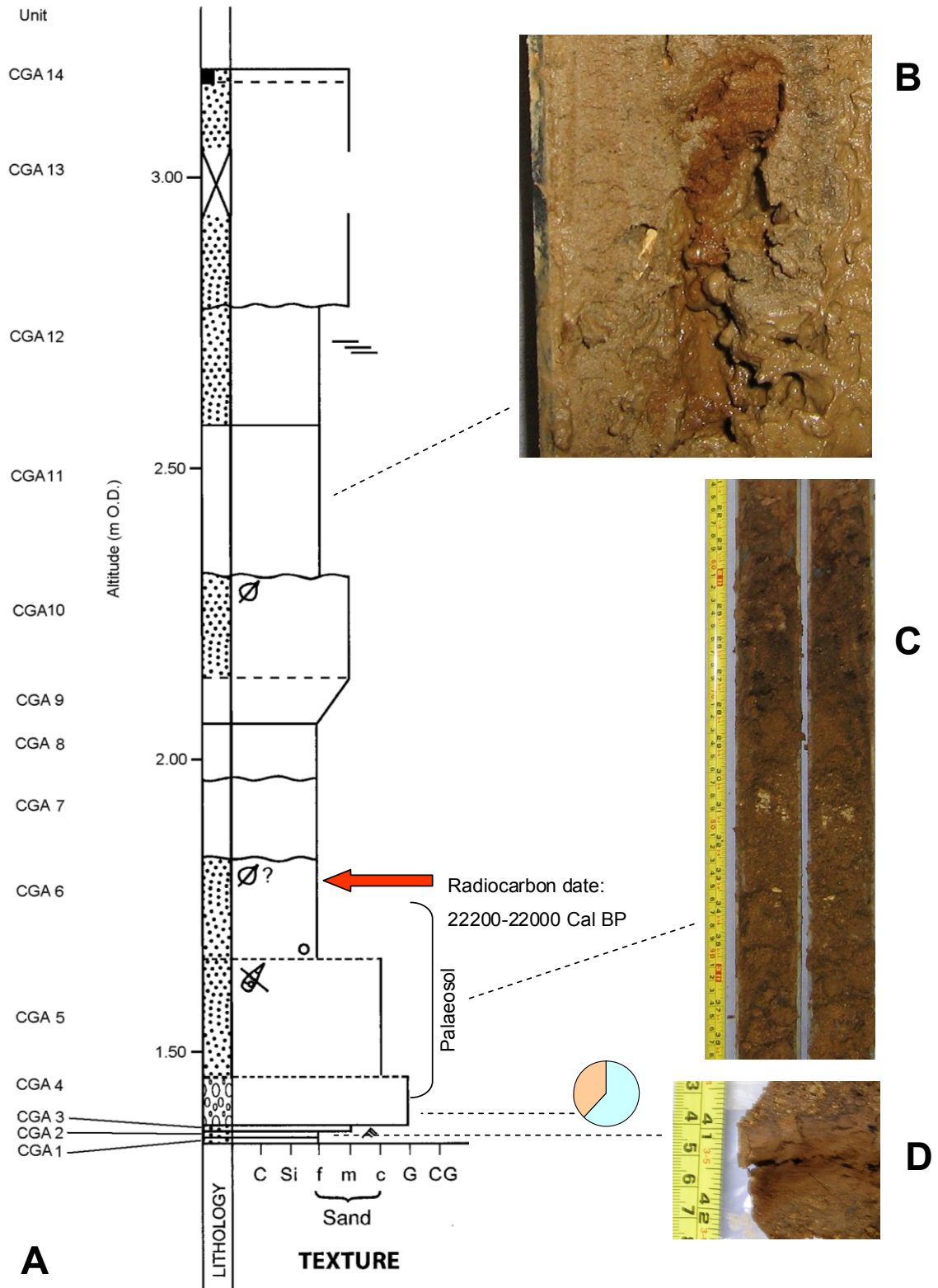


Figure 6.3: A. Stratigraphy of core CGA; stratigraphic units are shown on the left. B. Detail of iron stained root trace in CGA11. C. Palaeosol horizons of CGA4, CGA5 and CGA6 which become darker with increasing altitude. D. Rippled sand in CGA2

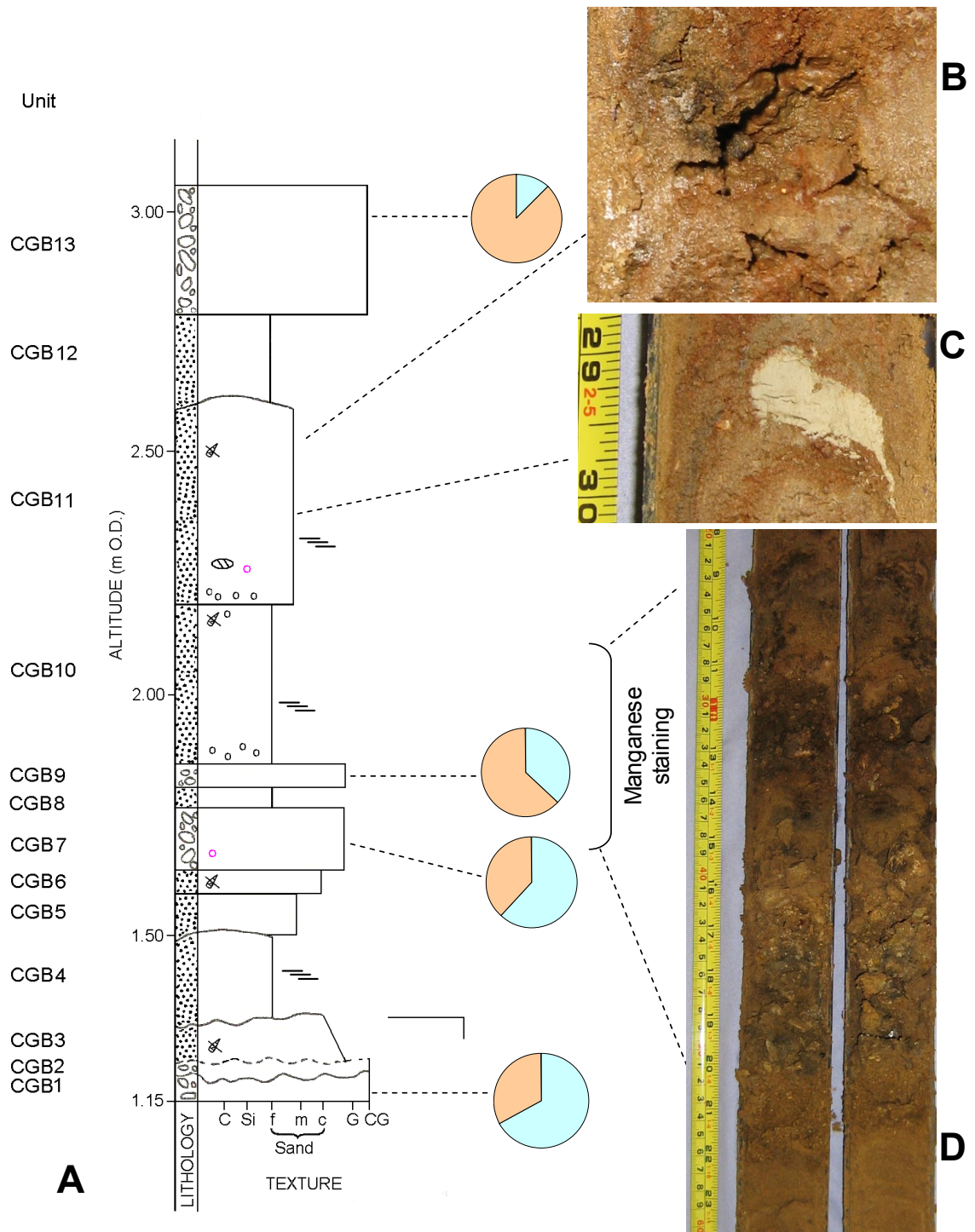


Figure 6.4: A. Stratigraphy of core CGB; stratigraphic units are shown on the left. B. Detail of void in CGB11. C. Soft carbonate nodule and Liesegang rings in CGB11. D. Dark staining of gravel clasts in CGB7, CGB8, CGB9 and CGB10

A number of boundaries are convex or contorted; that between CGB3 and CGB4 is both irregular and convoluted. The convex-up boundary between CGB4 and CGB5 is probably a coring-induced structure (Evans & Benn 2004), whereas the convex-up boundary between CGB12 and CGB11 is unlikely to be coring-induced because the boundaries above and below it are both planar, suggesting that this is a reactivation surface (Allen 1982, Maddy *et al.* 1998).

CGB11 contains a sub-vertical void (Figure 6.5B) which measures 22 mm x 12 mm x 17 mm and has a generally smooth internal surface, but displays pelleting in the upper right of the void. There appears to be little distortion of the void, indicating limited sediment compaction. Iron mottling is found in CGB13 and CGB11, where it is strongly associated with root traces and small carbonate nodules (<1 cm long) which have diffuse boundaries with the host sediment. CGB11 also displays Liesegang rings throughout its length. These have been deflected around a large white soft carbonate nodule, approximately 2 cm long (Figure 6.5C). This has a sharp boundary with its host sediment and a slightly irregular outline, probably coring-induced. In addition, CGB7 contains a number of carbonate nodules, all of which exhibit desiccation cracks; Figure 6.5 illustrates a typical example.

A number of units display indications of manganese deposition (Figure 6.5D), in particular black nodules and patches of dark mottled sediment in CGB10, dark mottling in CGB8 and CGB9 and black concretions and blackened pebbles in CGB7.

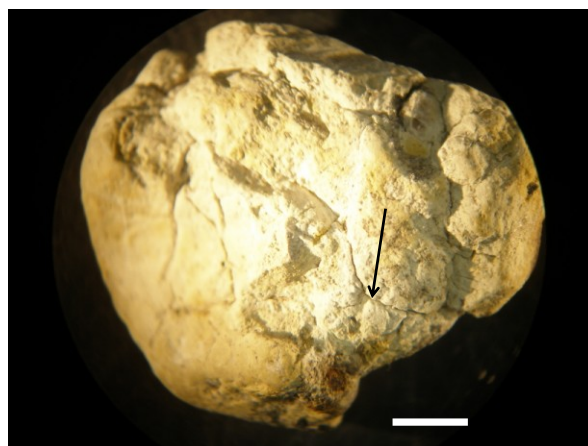


Figure 6.5: Typical carbonate nodule from CGB7 showing incipient desiccation cracks (arrowed).

Scale bar 2 mm

6.2.5 Stratigraphy of core NR

The stratigraphic log of core NR is illustrated in Figure 6.6. The boundaries between units are a mix of gradational and sharp, although there are more sharp boundaries than gradational. Four of the boundaries (Figure 6.6A) coincide with the base of a section of core and are unclear, but appear to be gradational. The sharp boundaries are both planar and irregular; the irregular boundaries are all in the upper part of the core, between NR16 and NR24. Three sharp boundaries, between NR20 and NR21, NR15 and NR16 and NR9 and NR10 are unconformable.

Two units, NR25 and NR19, contain *in situ* organic material; in NR25 these comprise the remains of a stem (Figure 6.6B) and a root, whilst NR19 contains a root. All are vertically oriented; however, the evidence of this material is incomplete as in both units the core cuts through the organic material.

Soft white carbonate nodules were found in NR20, NR22, NR24 and NR25 (Figure 6.6B). There is also a sequence of units indicating evidence of pedogenesis: the changes between NR13, NR14 and NR15 (Figure 6.6C) show similarities to a soil profile, with gradational boundaries between the units and increasingly darker colour with increasing altitude.

6.2.6 Stratigraphy of core CM

The stratigraphic log of core CM is illustrated in Figure 6.7. Most boundaries between units are sharp and irregular; the boundary between CM8 and CM9 is sharp and planar, between CM1 and CM2 is sharp and dipping and between CM12 and CM13 is sharp and convex-up. Three boundaries are gradational: between CM10 and CM11, between CM7 and CM8 and the irregular boundary between CM11 and CM12. The convex-up boundary between CM12 and CM13 could be a coring-induced structure (Evans & Benn 2004); however, the boundaries above and below it are both planar, suggesting the boundary represents a reactivation surface (Allen 1982, Maddy *et al.* 1998).

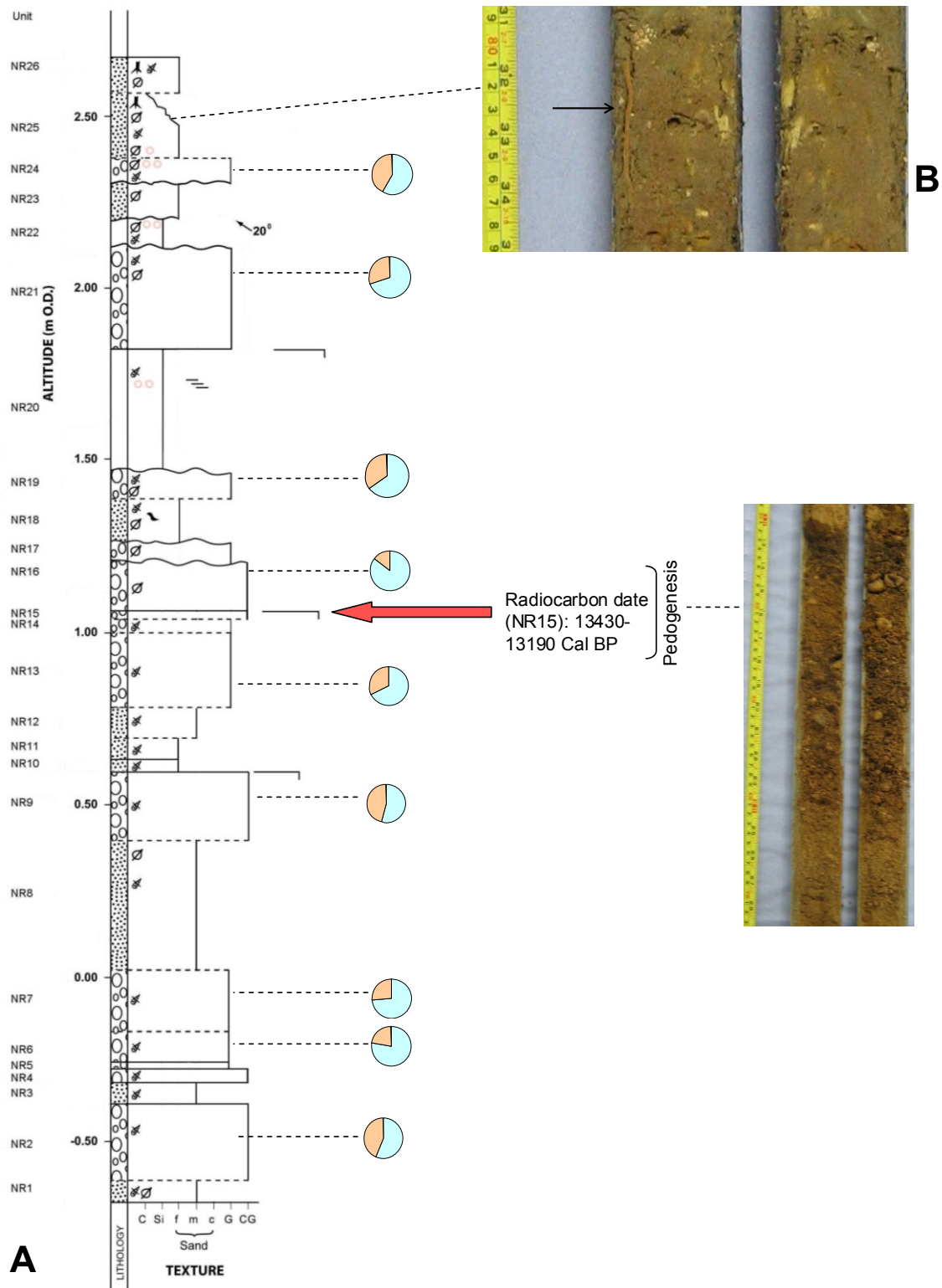


Figure 6.6: A. Stratigraphy of core NR; stratigraphic units are shown on the left. Boundaries between NR25 and NR24, NR19 and NR18, NR9 and NR8 and NR2 and NR1 are unclear and have been assigned gradational status on the basis of available evidence. B. Carbonate nodules and *in situ* organic remains (arrowed) in NR25. C. Pedogenesis in NR13, NR14 and NR15, showing increasingly darker colour with increased altitude

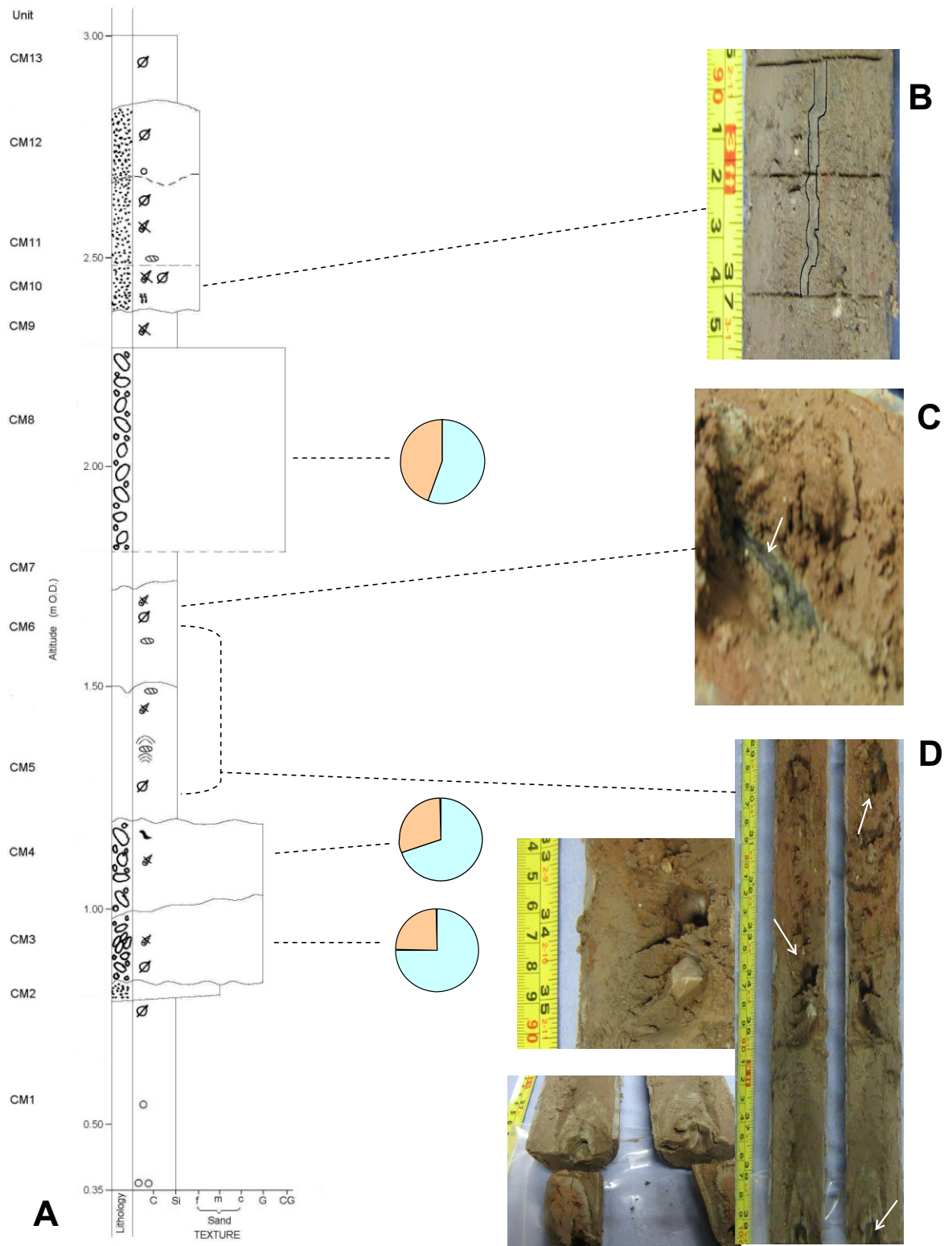


Figure 6.7: A. Stratigraphy of core CM; stratigraphic units are shown on the left. B. Bioturbation structure (outlined in black), subsequently infilled with finer material in CM10. C. Black organic material, probably a reed stem (white arrow) in CM6. D. Setting of voids in CM5 and CM6 (white arrows) and detail of voids in CM5; upper void showing smooth internal surface and angular stone below it; a bioturbation trace lies out of sight behind the stone. Lower void surrounded by greenish grey flame-shaped laminations

In CM10 a bioturbation trace, possibly an infilled root trace, forms an irregular line of finer material (Figure 6.7B), 2 mm wide and 6 mm long, which runs vertically down the unit with a nearby, but apparently unconnected void. A similar bioturbation feature occurs in CM5. CM6 contains blackened vertically oriented organic material; probably carbonised reed stems (Figure 6.7C).

A number of roughly spheroidal and internally smooth voids, possibly ichnofossils, are found in CM (Figure 6.7D). The void in CM11 (approximate dimensions 10 mm x 10 mm) has a stone positioned immediately below the void and light greenish grey (Gley1 7/1 10Y) base material that contains a shell fragment; the void in CM10 has approximately the same dimensions as that in CM11 (10 mm x 10 mm). However, the void in CM6 is larger (20 mm x 9 mm) and the overlying sediment has a dark colouration. CM5 has two voids; the upper is the larger (approximate dimensions 12 mm x 16 mm) and has a single angular large pebble-sized stone underneath it. A smooth-lined bioturbation trace (length 7 mm x width 3 mm) lies below the void and beneath the stone. The smaller lower void (approximate dimensions: length 10 mm x width 10 mm x depth 7 mm) coincides with the base of a core section and is surrounded by greenish grey (Gley1 6/1 5GY) flame-shaped haloes of sub-mm thickness.

Gravel unit CM3 contains a cluster of high-angle imbricated rounded gravel clasts (Figure 6.8). Imbrication is prominent because of the bladed/elongate morphology of the pebbles.



Figure 6.8 High-angle imbricated gravel of CM3. Arrow shows direction of imbrication

6.2.7 Stratigraphy of core TG

The stratigraphic log of core TG is illustrated in Figure 6.9. Boundaries between units above TG16 are all gradational; the basal contact of TG16, which coincides with the base of a core section, is unclear. Below TG16 the boundaries are sharp and either planar or slightly irregular due to a transition from or to gravel. Exceptions are the base of TG11, which is slightly convex and grades into laminations of the underlying unit, the boundary between TG4 and TG5 which is flame-shaped and the boundary between TG7 and TG8, which is sharp, planar and unconformable (Figure 6.9D).

Upper units have a large organic component; in TG18, this alternates with a minerogenic component (Figure 6.9B). TG8 and TG7 contain *in situ* fossil material; TG8 contains numerous molluscs throughout the unit, whilst the base of TG7 has whitish horizontally oriented organic fragments. TG10 displays laminations of sand and silt throughout its length (Figure 6.9C), some of which are rippled and iron-stained. TG2 is a coarse gravel of very weathered rounded large and small pebble-size clasts embedded in dense silt (Figure 6.9D). Weathering appears to increase downwards and stone content diminishes abruptly on transition to underlying unit.

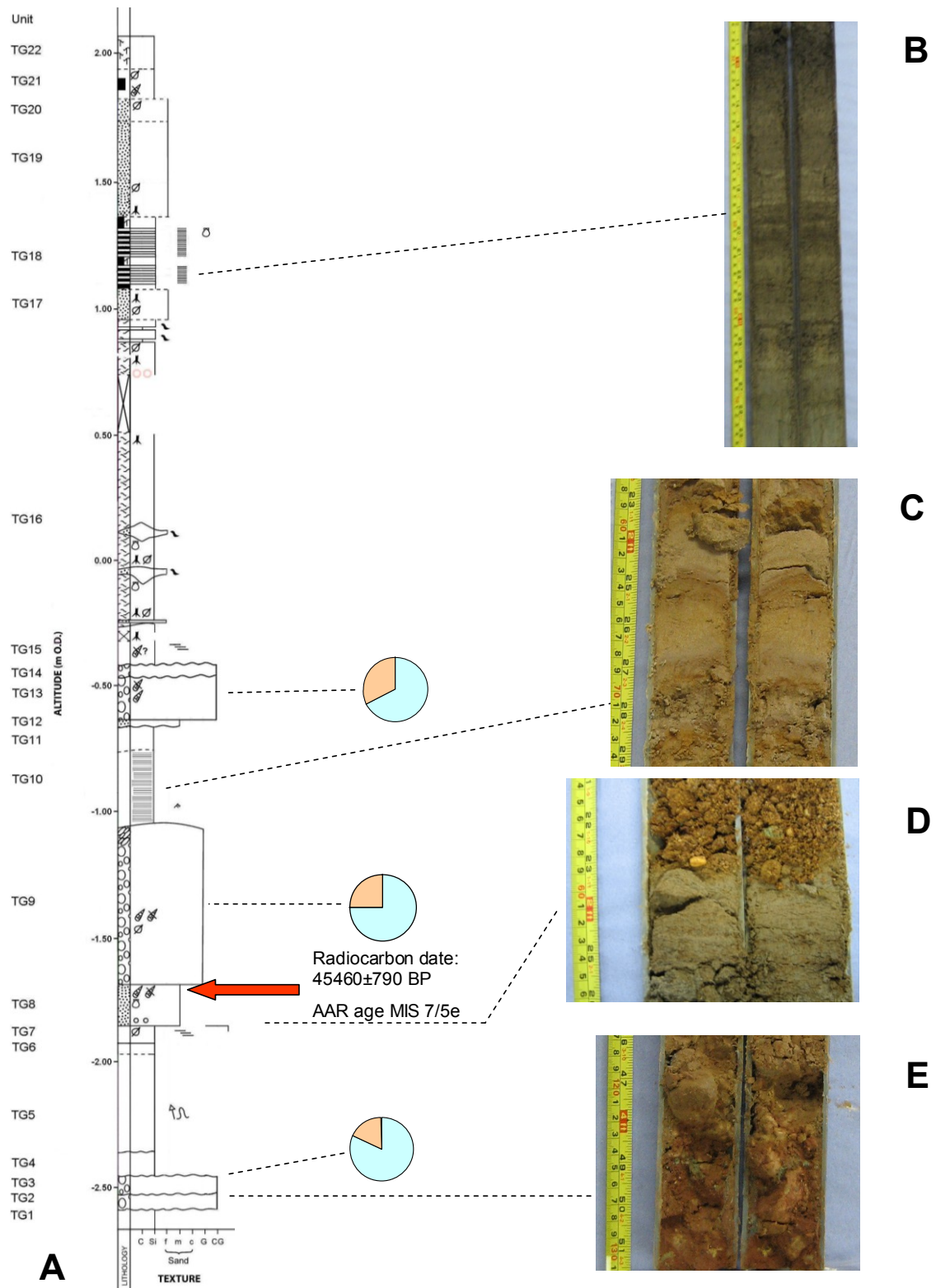


Figure 6.9: A. Stratigraphy of core TG; stratigraphic units are shown on the left. B. Thinly bedded organic and minerogenic sediments in TG18. C. Laminated fine sand and silt of TG10 and detail of iron-stained ripples. D. Transition from shelly sands of TG8 to grey silt of TG7. E. Weathered coarse gravel of TG2

6.3 Particle size analysis

Particle size analysis was carried out on all units identified during stratigraphic analysis using the techniques described in section 4.7.4; full details of particle size data and particle size distribution histograms are provided in Appendix III. Variations in the relative proportions of gravel, sand, silt and clay confirm that the cores are composed of a number of different sedimentary units which overall are very poorly sorted.

Results for core PG, summarised in Table 6.2, show that particle size ranges from *c.* 0.71 ϕ to 4.1 ϕ (coarse sand to very coarse silt), and all particle size distributions are multimodal. The sediments are mostly very poorly sorted ($\sigma_{\phi} = 2.8$ to 4.0 ϕ), although PG6 (silty gravel) is extremely poorly sorted ($\sigma_{\phi} = 4.7$ ϕ). Skewness ranges from symmetrical to coarse (0.3 to -0.8) and kurtosis from very platykurtic to mesokurtic ($K_{\phi} = 1.5$ to $K_{\phi} = 3.1$).

Table 6.2: Summary of particle size data for core PG

Unit	%	Gravel/Sand/Silt/Clay	Mode	Particle size distribution			
				Median particle size (ϕ)	Mean particle size (ϕ)	Sorting (σ_{ϕ})	Skewness (Sk_{ϕ})
PG8	23.52/52.71/22.48/1.11	Trimodal	1.903	1.875	3.147	-0.029	2.260
PG7	38.06/45.47/15.09/0.84	Trimodal	1.207	0.706	3.366	0.260	2.129
PG6	32.74/15.32/49.27/2.68	Bimodal	4.253	2.177	4.734	-0.462	1.545
PG5	17.99/29.17/49.19/3.66	Polymodal	4.519	3.386	3.714	-0.670	2.337
PG4	22.22/50.97/25.46/1.37	Polymodal	1.933	1.822	3.503	-0.286	2.363
PG3	13.94/24.72/57.75/3.28	Trimodal	4.746	3.270	3.252	-0.635	2.420
PG2	8.07/31.89/57.09/2.95	Trimodal	5.024	4.133	2.872	-0.825	3.116
PG1	12.95/54.47/30.56/1.93	Trimodal	2.708	2.879	2.911	-0.267	2.701

For core PGA (Table 6.3) mean particle size ranges from *c.* 0.6 ϕ to 5.5 ϕ (coarse sand to coarse silt); gravel clasts range from *c.* -2 ϕ to -5 ϕ (granules to large pebbles). Particle size distributions are mainly multimodal; exceptions are PGA5, PGA15, PGA16 and PGA17. The sediments are poorly or very poorly sorted ($\sigma_{\phi} = 1.1$ to 3.5 ϕ), with skewness ranging from very fine to very coarse (2.0 to -1.4) and kurtosis from platykurtic to very leptokurtic ($K_{\phi} = 2.0$ to $K_{\phi} = >7.4$).

Table 6.3: Summary of particle size data for core PGA

Unit	%	Gravel/Sand/Silt/Clay	Mode	Particle size distribution			
				Median particle size (ϕ)	Mean particle size (ϕ)	Sorting (σ_ϕ)	Skewness (Sk_ϕ)
PGA17	0.74/94.35/3.52/0.21	Unimodal	1.814	1.956	1.176	1.745	10.51
PGA16	2.28/90.69/5.86/0.36	Unimodal	1.791	2.019	1.394	1.586	9.030
PGA15	0.55/92.71/5.98/0.35	Unimodal	2.221	2.369	1.230	2.007	10.12
PGA14	31.42/46.20/21.02/1.21	Trimodal	1.748	1.372	3.524	-0.012	2.055
PGA13	12.56/17.79/65.73/3.91	Trimodal	5.473	4.553	2.943	-1.086	3.305
PGA12	18.05/28.64/49.89/3.15	Trimodal	4.534	3.597	3.392	-0.627	2.304
PGA11	9.71/25.93/60.04/4.11	Trimodal	5.319	4.321	3.111	-1.034	3.420
PGA10	3.10/21.44/70.57/4.89	Bimodal	5.790	5.158	2.428	-1.168	4.340
PGA9	13.40/36.94/46.31/2.63	Polymodal	3.891	3.349	3.352	-0.471	2.145
PGA8	17.27/61.03/20.14/1.11	Trimodal	2.189	2.182	2.729	0.116	2.570
PGA7	18.58/45.43/33.50/2.12	Polymodal	2.793	2.735	3.278	-0.304	2.239
PGA6	0.38/35.56/59.87/3.96	Bimodal	5.321	4.924	2.036	-0.259	2.493
PGA5	2.05/13.58/79.88/4.50	Unimodal	5.821	5.553	1.902	-1.404	6.628
PGA4	1.94/56.80/38.60/2.33	Bimodal	3.348	3.709	2.470	0.087	2.133
PGA3	31.18/44.02/23.26/1.31	Polymodal	1.436	1.462	3.422	0.212	1.996
PGA2	32.66/51.36/15.00/0.73	Trimodal	-0.321	0.635	2.881	0.962	2.994
PGA1	25.27/64.84/9.24/0.47	Trimodal	0.856	1.009	2.362	0.728	3.314

Mean particle size in core CGA, summarised in Table 6.4, ranges from *c.* -1.6 ϕ to 4.3 ϕ (medium gravel to coarse sand); gravel clasts in CGA4 varied from *c.*-1 ϕ to -5 ϕ (granules to large pebbles). Except for CGA13 and CGA14, particle size distributions are multimodal. The sediments are very poorly sorted ($\sigma_\phi = 1.0$ to 3.8 ϕ). Poorest sorting occurs in gravel unit CGA4, sand unit CGA6 and silt units CGA7, CGA8 and CGA11; CGA14 (poorly sorted) has best sorting. Skewness ranges from very fine to very coarse (4.5 to -0.76) and kurtosis from platykurtic to very leptokurtic ($K_\phi = 2.1$ to $K_\phi = >7.4$).

For core CGB (Table 6.5) mean particle size ranges from *c.* -1.2 ϕ to 4.1 ϕ (very fine gravel to very coarse silt) and all particle size distributions are multimodal. Most units are very poorly sorted ($\sigma_\phi = 1.9$ to 4.1 ϕ); CGB5 is poorly sorted and CGB13 is extremely poorly sorted, with skewness ranging from fine to coarse (1.1 to -0.6) and kurtosis from platykurtic to mesokurtic ($K_\phi = 1.8$ to $K_\phi = 3.7$).

Table 6.4: Summary of particle size data for core CGA

Unit	%	Gravel/Sand/Silt/Clay	Mode	Particle size distribution			
				Median particle size (ϕ)	Mean particle size (ϕ)	Sorting (σ_ϕ)	Skewness (Sk_ϕ)
CGA14	0.00/92.37/2.93/0.14	Unimodal	0.564	0.749	1.030	4.528	26.39
CGA13	10.96/75.12/12.18/0.69	Unimodal	1.999	2.045	2.248	-0.055	4.233
CGA12	14.60/56.50/26.45/1.67	Polymodal	2.549	2.621	2.901	-0.185	2.662
CGA11	15.96/38.27/41.56/2.90	Trimodal	3.585	3.446	3.127	-0.460	2.368
CGA10	8.66/58.17/30.57/2.21	Trimodal	2.577	3.005	2.724	-0.003	2.651
CGA9	3.28/42.33/50.21/3.35	Bimodal	4.833	4.294	2.562	-0.602	3.292
CGA8	13.63/37.12/46.02/2.87	Trimodal	3.903	3.411	3.349	-0.751	2.799
CGA7	18.85/36.65/41.83/2.04	Trimodal	3.575	2.831	3.781	-0.765	2.525
CGA6	27.56/47.99/22.67/1.17	Trimodal	1.201	1.216	3.550	0.056	2.105
CGA5	21.15/62.43/14.98/0.85	Trimodal	1.137	1.109	2.976	0.208	2.895
CGA4	65.56/27.92/5.65/0.26	Bimodal	-3.089	-1.587	3.088	1.040	3.142
CGA3	11.82/50.13/34.55/2.83	Trimodal	2.268	2.964	2.987	0.074	2.111
CGA2	9.71/52.76/35.84/1.38	Trimodal	3.502	3.258	2.767	-0.623	3.170
CGA1	4.47/63.43/30.83/1.28	Bimodal	3.495	3.590	2.151	-0.268	3.607

Table 6.5: Summary of particle size data for core CGB

Unit	%	Gravel/Sand/Silt/Clay	Mode	Particle size distribution			
				Median particle size (ϕ)	Mean particle size (ϕ)	Sorting (σ_ϕ)	Skewness (Sk_ϕ)
CGB13	46.59/37.02/15.20/0.99	Trimodal	0.916	-0.120	4.131	0.200	1.780
CGB12	7.40/55.73/34.46/2.41	Bimodal	3.082	3.383	2.715	-0.280	2.953
CGB11	5.31/52.33/39.26/2.59	Bimodal	3.447	3.741	2.575	-0.283	2.901
CGB10	7.55/66.25/24.44/1.27	Trimodal	2.517	2.787	2.542	-0.211	3.555
CGB9	33.00/49.94/16.38/0.61	Trimodal	1.395	0.882	3.260	0.143	2.137
CGB8	14.94/70.46/13.46/0.72	Bimodal	2.400	2.040	2.691	-0.581	3.559
CGB7	53.67/34.18/11.26/0.66	Trimodal	-1.944	-0.494	3.586	0.591	2.194
CGB6	2.82/75.70/19.80/1.23	Bimodal	2.069	2.576	2.173	0.788	3.496
CGB5	0.26/75.59/21.69/1.92	Bimodal	2.657	3.307	1.914	1.145	3.689
CGB4	0.11/59.32/36.69/3.51	Bimodal	3.169	4.080	2.173	0.519	2.175
CGB3	29.75/48.92/20.26/0.82	Trimodal	0.827	0.972	3.383	0.301	2.146
CGB2	57.11/34.41/8.03/0.53	Bimodal	-2.082	-1.150	3.303	0.867	2.975
CGB1	63.87/20.46/13.07/0.60	Trimodal	-2.679	-1.266	3.661	1.078	2.982

Results for core NR, summarised in Table 6.6, show that mean particle size ranges from *c.* -2.5 ϕ to 4.3 ϕ (fine gravel to very coarse silt); gravel clasts range from *c.* -1 ϕ to -6 ϕ (granule to very large pebble size). Most particle size distributions are multimodal; exceptions are NR1, NR2, NR9, NR10, NR11 and NR12. The sediments are poorly to extremely poorly sorted ($\sigma_\phi = 1.6$ to 4.3 ϕ), with skewness ranging from very fine to coarse (2.1 to -1.0) and kurtosis from very platykurtic to very leptokurtic ($K_\phi = 1.5$ to $K_\phi = >7.4$).

Table 6.6: Summary of particle size data for core NR

Unit	%	Particle size distribution					
		Gravel/Sand/Silt/Clay	Mode	Median particle size (ϕ)	Mean particle size (ϕ)	Sorting (σ_ϕ)	Skewness (Sk_ϕ)
NR26	0.13/72.15/25.33/1.71	Bimodal	2.743	3.372	2.032	0.844	2.811
NR25	17.10/60.62/20.24/1.52	Trimodal	2.316	2.037	3.277	-0.460	2.869
NR24	38.67/31.99/27.17/2.16	Trimodal	1.973	1.206	4.289	0.007	1.563
NR23	18.06/62.66/17.20/1.54	Trimodal	2.213	2.014	3.021	-0.174	2.758
NR22	15.70/35.52/45.14/3.60	Trimodal	3.860	3.282	3.815	-0.787	2.643
NR21	39.56/43.05/14.84/1.72	Trimodal	1.529	0.489	4.030	0.108	1.776
NR20	8.61/31.36/55.42/4.23	Trimodal	5.229	4.332	3.001	-1.000	3.583
NR19	30.98/35.37/30.69/2.66	Trimodal	2.035	1.901	3.870	0.019	1.678
NR18	26.66/38.92/31.04/2.57	Polymodal	2.532	2.138	3.932	-0.292	1.946
NR17	34.46/25.21/37.71/2.35	Trimodal	2.766	1.932	4.240	-0.181	1.486
NR16	70.74/21.75/6.58/0.76	Bimodal	-4.265	-2.482	3.791	1.196	3.272
NR15	69.53/21.80/7.96/0.74	Bimodal	-4.235	-2.084	3.707	1.233	3.183
NR14	59.18/29.82/9.63/0.76	Bimodal	-2.312	-0.831	3.204	1.148	3.382
NR13	39.74/50.04/8.74/0.25	Trimodal	0.114	-0.704	2.938	0.549	2.868
NR12	4.83/83.05/10.61/0.84	Unimodal	1.979	2.207	1.927	0.466	5.866
NR11	0.00/86.39/12.19/1.23	Unimodal	2.668	3.038	1.553	1.583	6.234
NR10	0.15/83.07/14.85/1.51	Unimodal	2.434	2.762	1.900	1.201	4.382
NR9	73.54/15.92/4.92/0.50	Unimodal	-3.629	-2.309	3.116	1.635	4.785
NR8	23.80/63.83/11.30/1.07	Bimodal	1.409	1.058	3.002	0.044	2.926
NR7	42.66/47.25/8.78/0.81	Trimodal	0.318	0.040	3.138	0.452	2.630
NR6	66.87/27.44/4.67/0.49	Bimodal	-2.748	-1.287	2.908	1.254	3.732
NR5	44.50/46.20/7.68/0.69	Bimodal	1.074	-0.004	3.230	0.388	2.205
NR4	66.76/29.63/3.25/0.29	Bimodal	-3.200	-1.806	3.101	0.936	2.846
NR3	15.19/77.30/5.79/0.53	Bimodal	1.577	1.300	2.245	-0.192	4.602
NR2	84.21/12.94/2.56/0.23	Unimodal	-3.725	-1.850	2.506	2.149	7.410
NR1	4.34/85.69/9.18/0.89	Unimodal	1.583	1.862	1.876	1.342	5.808

Results for core CM (Table 6.7) show that mean particle size ranges from *c.* -1.0 ϕ to 5.2 ϕ (very fine gravel to coarse silt) and all the particle size distributions are multimodal. The sediments are mostly very poorly sorted ($\sigma_\phi = 2.3$ to 3.8 ϕ), although CM4 and CM8 are extremely poorly sorted ($\sigma_\phi = c.$ 4.1 ϕ) and CM11 is poorly sorted ($\sigma_\phi = 1.9$ ϕ). Skewness ranges from fine to very coarse (1.1 to -2.1) and kurtosis from very platykurtic to very leptokurtic ($K_\phi = 1.7$ to $K_\phi = >7.4$).

Table 6.7: Summary of particle size data for core CM

Unit	%	Particle size distribution					
		Gravel/Sand/Silt/Clay	Mode	Median particle size (ϕ)	Mean particle size (ϕ)	Sorting (σ_ϕ)	Skewness (Sk_ϕ)
CM13	0.83/37.22/58.09/3.44	Bimodal	5.369	4.755	2.275	-0.509	2.992
CM12	7.00/63.01/27.93/1.54	Trimodal	2.668	2.957	2.758	-0.591	4.088
CM11	1.42/79.39/17.60/1.38	Bimodal	2.500	2.938	1.948	0.851	4.276
CM10	11.17/59.65/26.96/2.14	Trimodal	2.662	2.891	2.898	-0.307	3.038
CM9	28.55/33.12/35.98/2.34	Trimodal	2.143	2.182	3.843	-0.095	1.665
CM8	45.02/32.85/20.34/1.41	Trimodal	1.033	0.390	4.091	0.284	1.742
CM7	9.07/28.36/59.15/3.46	Trimodal	5.188	4.207	2.989	-0.968	3.339
CM6	17.87/22.12/55.63/4.29	Trimodal	5.457	3.777	3.777	-0.722	2.185
CM5	9.41/23.06/63.10/4.44	Trimodal	5.535	4.436	3.367	-1.430	4.491
CM4	46.11/33.30/19.11/1.41	Trimodal	0.263	0.242	4.111	0.365	1.773
CM3	62.25/29.48/7.51/0.48	Bimodal	-2.768	-1.039	3.118	1.067	3.097
CM2	27.50/56.85/14.22/1.44	Polymodal	1.106	0.960	3.140	0.396	2.721
CM1	3.97/12.89/80.05/3.08	Bimodal	5.830	5.229	2.502	-2.061	8.034

For core TG (Table 6.8) mean particle size ranges from *c.* -3.1 ϕ to 5.9 ϕ (medium gravel to coarse silt); gravel clasts range from *c.* -1 ϕ to -5 ϕ (granule to large pebble size). Particle size distributions are mostly multimodal; exceptions are TG1, TG2, TG3, TG7, TG14 and TG22. The sediments are poorly to extremely poorly sorted ($\sigma_\phi = 1.3$ to 4.8 ϕ), with skewness ranging from very fine to coarse (2.5 to -2.4) and kurtosis from very platykurtic to very leptokurtic ($K_\phi = 1.6$ to $K_\phi = >7.4$).

Table 6.8: Summary of particle size data for core TG

Unit	%	Gravel/Sand/Silt/Clay	Particle size distribution				
			Mode	Median particle size (ϕ)	Mean particle size (ϕ)	Sorting (σ_ϕ)	Skewness (Sk_ϕ)
TG22	0.00/6.20/88.88/3.54	Unimodal	6.026	5.941	1.302	-0.458	4.409
TG21	0.00/32.01/64.08/3.92	Bimodal	5.280	5.129	1.735	-0.005	2.645
TG20	5.88/56.77/34.95/2.27	Bimodal	3.711	4.047	2.185	-0.595	4.522
TG19	0.00/51.44/45.85/1.59	Bimodal	3.947	4.662	1.495	0.665	2.560
TG18	0.00/24.35/71.79/4.47	Bimodal	5.435	5.318	1.525	0.081	3.228
TG17	0.00/53.27/44.03/2.35	Bimodal	3.915	4.635	1.632	0.582	2.727
TG16	0.00/18.73/76.12/4.93	Bimodal	5.806	5.644	1.590	-0.226	3.016
TG15	29.99/9.54/56.22/4.25	Bimodal	5.103	2.693	4.840	-0.592	1.654
TG14	72.26/13.84/12.83/1.08	Unimodal	-3.660	-1.839	3.769	1.385	3.557
TG13	55.42/13.68/28.46/2.35	Bimodal	-2.407	-0.132	4.744	0.519	1.600
TG12	21.69/63.21/13.64/1.06	Bimodal	1.301	1.141	2.840	0.351	3.180
TG11	2.08/32.06/59.91/5.95	Trimodal	5.586	4.752	2.719	-0.620	2.491
TG10	3.60/43.83/48.82/3.39	Bimodal	4.290	4.587	2.275	-1.107	6.086
TG9	59.91/33.61/5.71/0.51	Bimodal	-2.397	-1.350	3.108	0.909	3.359
TG8	16.66/67.11/9.82/0.71	Bimodal	1.124	1.147	2.352	0.665	4.101
TG7	0.41/17.55/75.54/5.58	Unimodal	5.811	5.609	1.759	-0.665	4.543
TG6	0.00/15.92/77.60/6.47	Bimodal	6.060	5.831	1.696	-0.640	3.810
TG5	0.00/16.34/76.94/5.41	Bimodal	5.752	5.697	1.507	0.085	2.677
TG4	0.00/19.69/73.97/4.61	Bimodal	5.493	5.498	1.514	0.260	2.576
TG3	87.29/5.25/6.63/0.44	Unimodal	-4.228	-3.104	2.953	2.498	8.184
TG2	74.75/3.76/20.35/1.07	Unimodal	-4.128	-1.679	4.336	1.222	2.755
TG1	3.95/7.32/84.21/3.94	Unimodal	6.007	5.560	2.279	-0.383	10.09

6.4 Lithology of gravel clasts

Results of clast lithological analysis, carried out on all clasts in the -2 to -5 ϕ size fraction of gravel units using the methods discussed in section 4.8, are summarised in Table 6.9; full details, including data for units with low clast numbers in the relevant size fraction, are provided in Appendix IV. Most of the gravels are predominantly limestone, in the case of NR16 and TG3 overwhelmingly so (>80%). However, PG7, PGA14, CGB9 and CGB13 are predominantly brown sandstone and NR9 and CM8 have relatively large components of brown sandstone (30.27% and 26.22% respectively).

Table 6.9: Clast lithological analysis of gravel units based on percentages of the -2 to -5 ϕ fraction

Unit	Local				Exotics				N° of clasts
	Limestone %	Brown sandstone %	Other local %	Total %	Quartz & quartzite %	Flint %	Other exotics %	Total %	
PG7	22.32	50.00	13.39	85.71	11.61	0.89	1.79	14.29	112
PGA14	27.00	54.33	14.17	95.50	3.83	0.67	0.00	4.50	600
CGA4	61.64	15.07	9.59	86.30	8.22	5.48	0.00	13.70	73
CGB 13	12.50	68.75	11.25	92.50	6.25	1.25	0.00	7.50	80
CGB9	37.04	42.59	11.11	90.74	7.41	1.85	0.00	9.26	54
CGB7	61.59	15.23	15.24	92.06	5.29	2.65	0.00	7.94	151
CGB1	67.01	18.55	5.17	90.73	5.15	4.12	0.00	9.27	97
NR24	58.06	16.13	9.68	83.87	16.13	0.00	0.00	16.13	31
NR21	69.64	16.07	14.29	100.00	0.00	0.00	0.00	0.00	56
NR19	64.86	18.93	16.22	100.00	0.00	0.00	0.00	0.00	37
NR16	85.37	7.32	4.87	97.56	0.00	2.44	0.00	2.44	41
NR13	67.47	18.07	4.82	90.36	4.82	4.82	0.00	8.42	83
NR9	54.13	30.27	10.10	94.50	1.83	0.92	2.75	5.50	109
NR7	73.13	13.43	10.45	97.01	2.24	0.75	0.00	2.99	134
NR6	77.61	13.57	2.85	94.03	4.48	0.00	1.49	5.97	67
NR2	56.08	17.99	20.64	94.71	5.29	0.00	0.00	5.29	189
CM8	54.88	26.22	7.92	89.02	9.76	0.61	0.61	10.37	164
CM4	69.56	8.60	3.00	81.16	15.94	2.90	0.00	18.84	69
CM3	75.00	11.46	8.33	94.79	3.13	2.08	0.00	3.13	96
TG13	67.31	15.39	13.46	96.16	3.84	0.00	0.00	3.84	52
TG9	74.60	12.57	5.61	92.78	5.08	2.14	0.00	7.22	373
TG3	82.05	12.82	0.00	94.87	2.56	2.56	0.00	5.12	39

Most gravels have an exotic component comprising quartz and/or quartzite, although these are durable lithologies and could have been subjected to an extremely long transport history. However, no clasts of quartz or quartzite are recorded for NR24, NR21, NR19, NR6, NR2 and TG13. Many of the gravels also have a flint component; in CM4 this accounts for 18.84% of the total number of clasts. The gravels of core NR include clasts of goethite and ironstone.

Other exotic lithologies are present, although the small size of the rock fragments makes full identification difficult. These include a clast of dark grey-brown coarse sandstone with angular grains, possibly derived from Triassic New Red Sandstone and a dark grey-brown piece of granite in PG7, and a possibly exotic clast of pinkish grey coarse sandstone of well rounded grains with a red colour together with a variety of rock types, possibly cemented with kaolinite, identified as either a fragment of Triassic sandstone or weathered granite in CM8. NR6 has a possible iron pan clast; the clast has a lot of sand as host sediment, which would be exotic to Tickenham Ridge, the nearest source for gravel clasts. NR9 includes clasts of possible iron pan, a very dark grey, glassy rock fragment which is not dense enough to be basalt and may be tourmaline, although it lacks the striations often found on the long side of tourmaline crystals (Jones 2007) and a very dark greyish brown clast of coarse sandstone, possibly derived from weathered granite, that is almost a conglomerate of grains of very coarse sand to granule size, including a variety of rock types, possibly cemented by kaolinite.

In the gravel units with low clast numbers analysis of their lithology indicates that the majority of clasts are limestone, with a small component of quartz, quartzite and/or flint, although the majority of clasts in GV2 and PG6 are brown sandstone.

In addition, a small number of tufa clasts were recovered (Figure 6.10). PG6 contains a single tufa clast and a small number of tufa clasts were also recovered from PGA3, PGA14 and CM3. PGA14 also contains a carbonate concretion which exhibits a concentric, laminar internal structure. Formation appears to be focused on the mould of a gastropod shell. The internal structure and the depositional focus of the carbonate suggest that this is also a tufa clast rather than a carbonate concretion.

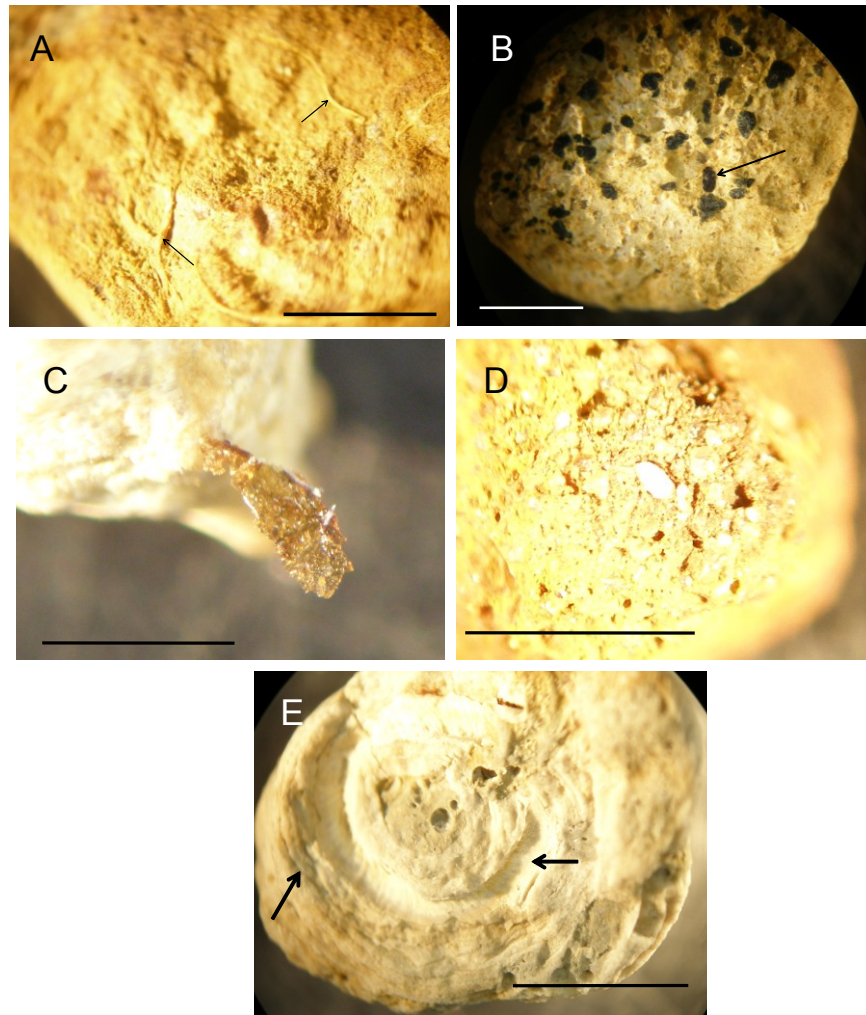


Figure 6.10: Tufa clasts from gravels of the Gordano Valley. A. Detail of tufa clast from PG6 showing incorporated plant material (arrowed). Scale bar 2 mm. B. Tufa clast from CM3. Dark areas appear to be incorporated organic material, including the mould of an ostracod (arrowed). Scale bar 1 mm. C. Tufa clast from PGA3 with organic material protruding from the clast. Scale bar 250 μm . D. Tufa clast from PGA14. Scale bar 1.75 mm. E. Internal laminar structure of carbonate concretion from PGA14 (arrowed left). Focus of concretion formation appears to be a gastropod shell (arrowed right). Scale bar 3 mm

6.5 Clast morphological analysis

Clast morphological analysis was applied to the -2 to -5 ϕ limestone fraction of gravel units using the techniques discussed in section 4.9; the results are summarised in Table 6.10. Full details of the gravel morphological analysis, including data for units with low clast numbers in the relevant size fraction, are provided in Appendix IV.

Table 6.10: Morphology, OPI and sphericity of limestone clasts
(after Sneed & Folk 1958, Dobkins & Folk 1970)

Unit	Morphology											Mean Sphericity	N° of clasts
	Compact	Compact-Platy	Compact-Bladed	Compact-Elongate	Platy	Bladed	Elongate	Very-Platy	Very-Bladed	Very-Elongate	Mean OPI		
PG7	13.51	18.92	16.22	8.11	13.51	13.51	5.41	2.70	5.41	2.70	-1.03	0.69	37
PGA14	7.08	10.42	15.42	8.33	14.58	27.08	7.50	4.58	4.58	0.42	-1.22	0.66	244
CGA4	1.72	1.72	18.97	13.79	15.52	25.86	12.07	8.62	1.72	0.00	-2.12	0.65	59
CGB13	0.00	8.11	16.22	13.51	8.11	29.73	8.11	8.11	8.11	0.00	-0.72	0.64	38
CGB7	4.71	1.18	16.47	16.47	9.41	28.24	11.76	2.35	9.41	0.00	0.40	0.67	85
CGB1	5.45	7.27	10.91	9.09	7.27	20.00	20.00	10.91	7.27	1.82	-0.01	0.64	55
NR21	3.33	0.00	10.00	13.33	6.67	20.00	26.67	10.00	10.00	0.00	0.31	0.64	30
NR16	5.71	11.43	14.29	5.71	20.00	25.71	8.57	5.71	0.00	2.86	-1.47	0.66	35
NR13	4.00	10.00	18.00	8.00	8.00	34.00	8.00	2.00	4.00	4.00	0.18	0.66	50
NR9	9.09	10.91	16.36	5.45	5.45	30.91	12.73	3.64	5.45	0.00	-0.34	0.68	55
NR7	2.38	9.52	15.48	13.10	15.48	21.43	9.52	4.76	7.14	1.19	-1.01	0.65	84
NR6	4.00	2.00	12.00	14.00	18.00	34.00	6.00	8.00	2.00	0.00	-2.44	0.64	50
NR2	3.09	10.31	10.31	13.40	17.53	21.65	10.31	7.22	4.12	2.06	-0.40	0.65	97
CM8	4.72	7.87	7.09	4.72	21.26	25.98	7.87	9.45	9.45	1.57	-2.64	0.61	128
CM4	1.89	13.21	7.55	7.55	11.32	32.08	15.09	5.66	3.77	1.89	-0.28	0.64	53
CM3	10.34	8.62	5.17	5.17	15.52	24.14	12.07	6.90	10.34	1.72	-0.95	0.64	59
TG13	8.82	5.80	17.65	5.88	8.82	14.71	11.76	14.71	11.76	0.00	-1.68	0.63	35
TG9	2.53	7.17	12.24	10.13	18.99	26.16	8.44	4.22	9.28	0.84	-1.35	0.64	241
TG3	0.00	3.23	12.90	29.03	9.68	25.81	12.90	6.45	0.00	0.00	0.27	0.69	31

For most gravels the dominant clast morphology is bladed and mean sphericity averages 0.65, ranging from 0.61 to 0.69. A small number of units have overall clast morphologies that differ. In PG7 the largest percentage of clasts are compact-platy and as a group the compact classes form the majority of clast morphologies (56.76%); mean sphericity of 0.69 also indicates an overall compact morphology. In CGB1 the largest percentage is in the bladed and elongate classes (20.00% in each), whilst in NR21 the largest percentage of clasts is elongate (26.67%). The largest percentage of clasts in TG3 is compact-elongate (29.03%); mean sphericity of 0.69 indicates an overall compact

morphology. Although the largest percentage of clasts in TG13 is compact-bladed (17.65%), there is a greater spread of shapes including relatively large percentages of very platy and very bladed clasts.

Of the gravel units with low clast numbers PGA2, CGB2, CGB9, NR4 and TG14 have predominantly bladed clasts; PGA3 and NR14 have mostly compact-elongate clasts; clasts in NR5 are mostly compact-bladed; most clasts in NR19 are platy; clasts in NR17 are compact-elongate/platy/very platy and for NR24 and TG2 most clasts are in the platy and bladed classes. The four clasts of NR15 each have a different morphology; compact-platy, compact-elongate, compact-bladed and bladed and the two clasts in PG6 are compact and platy.

Results of clast roundness analysis are summarised in Table 6.11. Most clasts are angular, although there is also a large proportion of sub-angular clasts. Only PG7, CGB7 and CM4 have no very angular clasts, PGA14, NR21, NR16, CM8, TG13 and TG3 have no round clasts and well round clasts are found only in CGB7, NR9 and TG9. The highest proportion of sub-angular clasts is found in CGB7 (37.63%) and NR13 (37.50%), whilst the lowest proportion is in TG3 (12.50%). The clasts of core NR are predominantly very angular to angular; NR21 has only very angular and angular clasts, and round and well round clasts are found only in units below NR13. All the gravels contain a small proportion of broken clasts, some of which show evidence of subsequent re-rounding. The highest proportions of broken clasts all occur in core TG, with the largest proportion in TG3 (31.25%), whilst NR21 has the lowest proportion (2.56%). In PG7 all the breaks appear fresh, indicating that breakage occurred during the last episode of transportation.

In the gravel units with low clast numbers, both limestone clasts in PG6 are sub-round. Most clasts in PGA2 and PGA3 are angular whereas in CGB2, CGB9 and CGB13 they are mainly sub-angular; CGB13 is one of only four units to contain any well round clasts. TG2 has very angular to sub-angular clasts and those of TG14 are angular and sub-angular.

Table 6.11: Roundness of limestone clasts (after: Powers 1953)

Unit	Roundness							N° of clasts
	% Very Angular	% Angular	% Sub-Angular	% Sub-Round	% Round	% Well Round	% Broken	
PG7	0.00	46.15	30.77	19.23	3.85	0.00	12.50	37
PGA14	18.40	60.74	16.56	4.29	0.00	0.00	7.36	163
CGA4	6.67	35.56	33.33	20.00	4.44	0.00	11.11	59
CGB13	10.00	30.00	50.00	10.00	0.00	0.00	0.00	10
CGB7	0.00	38.70	37.63	18.28	4.30	1.08	12.90	93
CGB1	3.13	32.81	31.25	21.88	9.38	1.56	10.94	64
NR21	58.97	41.03	0.00	0.00	0.00	0.00	2.56	39
NR16	5.71	45.71	34.29	14.29	0.00	0.00	11.43	35
NR13	3.57	39.29	37.50	17.86	1.79	0.00	10.71	56
NR9	11.86	45.76	22.03	16.95	1.69	1.69	13.56	59
NR7	11.22	39.80	31.63	16.33	1.02	0.00	7.14	98
NR6	13.46	44.23	25.00	15.38	1.92	0.00	3.85	52
NR2	15.89	43.93	23.36	15.89	0.93	0.00	14.15	107
CM8	14.44	52.22	24.44	8.89	0.00	0.00	5.56	90
CM4	0.00	29.79	36.17	29.79	4.26	0.00	8.51	47
CM3	2.78	36.11	33.33	23.61	4.17	0.00	18.06	96
TG13	5.71	40.00	34.29	20.00	0.00	0.00	22.86	35
TG9	9.32	38.71	21.15	23.30	6.81	0.72	20.07	279
TG3	37.50	34.38	12.50	15.63	0.00	0.00	31.25	32

6.6 Clast surface features

Surface features were assessed using the scheme set out in section 4.8.2 and their presence or absence recorded; results are shown in Table 6.12. The most common surface feature present is surficial white powdery deposits that reacted vigorously with dilute HCl, indicating the presence of calcium carbonate. These deposits are found on both limestone and sandstone clasts and are absent only in NR5, NR15 and TG14. Some clasts exhibit calcium carbonate deposits on one face only.

The next most common surface feature is pitting, mainly a feature of limestone clasts, but not wholly confined to them. This feature is absent from only PG6, PG7

(predominantly brown sandstone gravels, section 6.5), CGB2, NR15 and TG3. Cracks are common on limestone and sandstone clasts; additionally, a quartzite clast in NR24 has a surface crack and an ironstone clast in NR2 is criss-crossed by fine cracks. All carbonate nodules in CGB7 display desiccation cracks. Surface gouges are also common on both limestone and sandstone clasts; crescentic gouges are recorded on limestone clasts in NR13 and CM4. Striated surfaces are noted on limestone clasts in NR6, NR7, NR9, NR17, CM4, CM8 and TG3. A single siltstone clast of PGA2 demonstrates a polished surface, as do sandstone clasts of CGB1 and CM3 and a limestone and a quartzite clast of NR13. Chattermarks are found only on limestone clasts of TG9; an example is shown in Figure 6.11.

Table 6.12: Surface features of gravel clasts. X = present, O = absent

	Pitting	Gouges	Cracks	Surface polishing	Carbonate deposits	Striations	Chattermarks	Unit	Pitting	Gouges	Cracks	Surface polishing	Carbonate deposits	Striations	Chattermarks
PG6	O	O	O	O	X	O	O	NR13	X	X	X	X	X	O	O
PG7	O	O	X	O	X	O	O	NR14	X	O	O	O	X	O	O
PGA2	X	O	X	X	X	O	O	NR15	O	O	X	O	O	O	O
PGA3	X	O	X	O	X	O	O	NR16	X	X	O	O	X	O	O
PGA14	X	O	X	O	X	O	O	NR17	X	X	X	O	X	X	O
CGA4	X	O	X	O	X	O	O	NR19	X	X	O	O	X	O	O
CGB1	X	O	X	X	X	O	O	NR21	X	X	O	O	X	O	O
CGB2	O	O	O	O	X	O	O	NR24	X	X	O	O	X	O	O
CGB7	X	X	X	O	X	O	O	CM3	X	X	X	X	X	O	O
CGB9	X	O	X	O	X	O	O	CM4	X	X	X	O	X	X	O
CGB13	X	X	X	O	X	O	O	CM8	X	X	X	O	X	X	O
NR2	X	O	X	O	X	X	O	TG2	X	O	X	O	X	O	O
NR4	X	O	X	O	X	O	O	TG3	O	X	X	O	X	X	O
NR5	X	O	O	O	O	O	O	TG9	X	X	X	O	X	O	X
NR6	X	X	X	O	X	X	O	TG13	X	O	X	O	X	O	O
NR7	X	X	X	O	X	X	O	TG14	X	O	O	O	O	O	O
NR9	X	X	X	O	X	X	O								



Figure 6.11: Chattermarked limestone clast. Scale bar 2 mm

Results of the analysis of the weathered condition of gravel clasts are presented in Table 6.13. Full details of the weathered condition of gravel clasts are provided in Appendix IV. Most clasts display some evidence of weathering and there is a wide variety of weathering, even within the same unit. Most limestone clasts are slightly or moderately weathered, although limestone is also the only lithology to exhibit fresh clasts. However, in PGA14 and NR21 the limestone clasts are generally highly weathered. In those units where brown sandstone is the dominant lithology, limestone clasts are either slightly weathered (PG7) or highly weathered (CGB13). Brown sandstone clasts tend to display less evidence of weathering, generally being only slightly weathered, although more variable weathering is evident in CGB13 whilst the sandstones of other local lithologies (e.g. in PGA14) tend to be generally slightly weathered.

In the gravel units with low clast numbers analysis of their weathered condition shows moderate or high weathering of limestone clasts. Brown sandstone clasts in PG6 are moderately and highly weathered whereas in CGB9 (complete to slight) and NR19 (high to slight) weathering is more variable and in PGA2 and PGA3 brown sandstone and other local sandstone clasts are only slightly weathered.

Table 6.13: Weathered condition of clasts in gravel units based on percentages of the -2 to -5 ϕ fraction
(1 = Completely weathered; 5 = Fresh)

	1	2	3	4	5	N ^o of clasts
PG7						
Brown sandstone	0.00	14.29	5.36	80.36	0.00	56
PGA14						
Limestone	0.62	47.53	37.04	11.73	3.09	162
Brown sandstone	1.23	8.59	9.51	78.53	2.15	326
Other local sandstones	0.00	6.06	3.03	84.85	6.06	33
CGA4						
Limestone	0.00	13.33	48.89	35.56	2.22	45
CGB13						
Brown sandstone	3.64	23.64	34.55	32.73	5.45	55
CGB7						
Limestone	2.15	31.18	50.54	15.05	1.08	93
CGB1						
Limestone	0.00	7.69	58.46	32.31	1.54	65
NR21						
Limestone	0.00	41.03	20.51	35.90	2.56	39
NR16						
Limestone	0.00	14.29	54.29	28.57	2.86	35
NR13						
Limestone	0.00	5.36	81.43	23.21	0.00	56
NR9						
Limestone	0.00	3.39	33.90	62.71	0.00	59
Brown sandstone	0.00	3.03	3.03	93.94	0.00	33
NR7						
Limestone	0.00	7.14	48.98	40.82	3.06	98
NR6						
Limestone	0.00	5.77	48.08	40.38	5.77	52
NR2						
Limestone	0.00	0.94	30.19	66.98	1.89	106
Brown sandstone	0.00	23.53	8.82	67.65	0.00	34
CM8						
Limestone	0.00	10.00	28.89	48.89	12.22	90
Brown sandstone	0.00	16.28	25.58	58.14	0.00	43

Table 6.13 (continued): Weathered condition of clasts in gravel units based on percentages of the -2 to -5 ϕ fraction (1 = Completely weathered; 5 = Fresh)

	1	2	3	4	5	No of clasts
CM4						
Limestone	0.00	2.08	50.00	45.83	2.08	48
CM3						
Limestone	0.00	4.17	50.00	44.44	1.39	72
TG13						
Limestone	0.00	2.86	31.43	62.86	2.86	35
TG9						
Limestone	0.00	1.80	39.93	55.76	2.52	278
Brown sandstone	0.00	8.51	6.38	85.11	0.00	47
TG3						
Limestone	0.00	3.13	25.00	71.88	0.00	32

6.7 Geochemical analysis

Loss on ignition (section 4.7.3) was applied to the $>4 \phi$ fraction of all units. The percentages of weight loss are used as an indication of the percentage of organic and carbonate content of the individual sedimentary units and are summarised in Table 6.14. Organic content ranges from 0.39% to 21.58%, generally with a high of 2-3%, and carbonate content ranges from 0% to 39.26%.

In core PG the percentage of organic content ranges between 1.02% (PG1) and 2.46% (PG5) and the carbonate content ranges between 4.67% (slightly calcareous, PG6) and 8.97% (calcareous, PG7). Between PG1 and PG6 an increase in organic content coincides with an increase in carbonate content and conversely a decrease in organic content coincides with a decrease in carbonate content, whilst in PG7 a decrease in organic content corresponds with an increase in carbonate content and in PG8 a slight increase in organic content corresponds with a slight decrease in carbonate content. In core PGA the percentage organic content ranges between 0.40% (PGA2) and 2.04% (PGA12) and the percentage carbonate content ranges between 0.99% (very slightly calcareous, PGA17) and 14.14% (very calcareous, PGA2).

Table 6.14: Results for loss on ignition

Unit	%	%	Unit	%	%	Unit	%	%
	Organics	Carbonates		Organics	Carbonates		Organics	Carbonates
PG8	1.36	8.78	CGA14	0.67	0.00	NR26	1.49	7.26
PG7	1.25	8.97	CGA13	0.67	4.05	NR25	0.49	12.48
PG6	2.14	4.67	CGA12	0.83	6.65	NR24	1.33	5.48
PG5	2.46	6.57	CGA11	1.01	4.53	NR23	0.84	7.12
PG4	1.23	5.67	CGA10	0.84	5.34	NR22	1.99	4.65
PG3	2.02	7.05	CGA9	0.39	5.13	NR21	1.33	7.30
PG2	1.54	5.97	CGA8	1.84	3.51	NR20	2.18	3.69
PG1	1.02	5.75	CGA7	2.02	3.70	NR19	1.67	7.86
PGA17	0.50	0.99	CGA6	1.69	5.41	NR18	1.17	6.01
PGA16	0.82	1.64	CGA5	1.27	7.24	NR17	1.77	4.20
PGA15	0.50	2.65	CGA4	1.01	9.52	NR16	1.16	8.78
PGA14	0.83	7.83	CGA3	1.17	10.00	NR15	1.51	7.54
PGA13	2.03	3.73	CGA2	1.01	7.58	NR14	2.00	11.22
PGA12	2.04	5.79	CGA1	0.50	7.54	NR13	1.83	10.32
PGA11	2.03	5.41	CGB13	1.67	6.67	NR12	1.00	4.16
PGA10	1.87	6.81	CGB12	1.68	3.02	NR11	0.67	3.16
PGA9	1.18	7.39	CGB11	1.85	3.36	NR10	1.33	5.83
PGA8	0.67	5.32	CGB10	1.34	3.35	NR9	1.34	12.50
PGA7	0.67	7.00	CGB9	1.86	4.74	NR8	1.49	8.16
PGA6	0.49	5.97	CGB8	1.37	3.07	NR7	1.17	11.96
PGA5	1.01	4.39	CGB7	2.00	6.18	NR6	1.48	14.00
PGA4	0.84	7.05	CGB6	2.35	6.05	NR5	0.83	10.90
PGA3	1.36	10.17	CGB5	3.00	2.51	NR4	1.00	12.64
PGA2	0.40	14.14	CGB4	3.00	2.87	NR3	0.66	10.41
PGA1	1.19	11.49	CGB3	2.01	9.74	NR2	1.49	16.20
			CGB2	1.67	10.71	NR1	1.00	10.28
			CGB1	2.19	11.93			

Table 6.14 (continued): Results for loss on ignition

Unit	%	%	Unit	%	%	Unit	%	%
	Organics	Carbonates		Organics	Carbonates		Organics	Carbonates
CM13	2.86	1.01	TG22	8.73	39.26	TG11	2.01	14.89
CM12	1.00	4.64	TG21	11.34	31.64	TG10	1.83	19.47
CM11	1.33	4.31	TG20	8.74	7.73	TG9	1.16	17.30
CM10	1.83	5.33	TG19	21.30	15.61	TG8	0.99	17.69
CM9	2.16	8.97	TG18	21.58	24.36	TG7	2.85	11.83
CM8	1.83	8.62	TG17	3.15	9.19	TG6	2.69	12.44
CM7	2.17	6.86	TG16	4.81	9.12	TG5	1.50	13.00
CM6	3.59	9.40	TG15	3.33	8.84	TG4	2.00	12.15
CM5	2.34	6.03	TG14	1.81	13.30	TG3	1.84	15.89
CM4	2.84	8.52	TG13	2.00	10.63	TG2	3.84	8.73
CM3	2.00	10.83	TG12	1.00	9.45	TG1	2.63	10.35
CM2	1.82	10.43						
CM1	3.14	9.07						

In core CGA the percentage organic content ranges between 0.39% (CGA9) and 2.02% (CGA7), the higher values coinciding with those units which were identified from the stratigraphy as showing indications of pedogenesis. The percentage carbonate content ranges between 0% (CGA14) and 10.00% (CGA3), 'non-calcareous' to 'calcareous'. The carbonate content decreases in those units identified as showing indications of pedogenesis. Exceptionally, no carbonate content is recorded for CGA14. For core CGB the percentage organic content ranges between 1.37% (CGB8) and 3.00% (CGB4 and CGB5). The percentage carbonate content ranges between 2.51% (slightly calcareous, CGB5) and 11.93% (very calcareous, CGB1). The relatively high level of organic content in CGB4 and CGB5 coincides with a relatively low level of carbonate content.

In core NR the percentage organic content ranges between 0.49% (NR25) and 2.18% (NR20) and the percentage carbonate content ranges between 3.16% (slightly calcareous, NR11) and 16.20% (very calcareous, NR2). Between NR1 and NR15 changes in organic and carbonate content follow each other, with an increase in organic content coinciding with an increase in carbonate content and *vice versa*. This relationship changes between NR16 and NR26, when an increase in organic content coincides with a decrease in carbonate content and *vice versa*. In core CM the percentage organic content ranges

between 1.00% (CM12) and 3.59% (CM6) and the percentage carbonate content ranges between 1.01% (slightly calcareous, CM13) and 10.83% (very calcareous, CM3).

The largest values for organic and carbonate content are both found in core TG. The percentage organic content ranges between 0.99% (TG8) and 21.58% (TG18) and the percentage carbonate content ranges between 7.73% (calcareous, TG20) and 39.26% (very calcareous, TG22). Between TG1 and TG8 there appears to be an inverse relationship between organic and carbonate content; from TG9 upwards this relationship becomes more variable.

6.8 Redness

Redness ratings (section 4.12.2) for the sediments range between 0 and 25 and are shown in Table 6.15. In core PG, most of the sediments are brown, although PG5 is greenish grey, and redness ratings range from 7.50 for PG2 to 0.00 for PG1, PG3 and PG5. Only two units (PG2 and PG7) have redness ratings ≥ 5.00 . For core PGA, most sediments are red to yellowish brown and redness ratings range from 11.25 for PGA1 to 0.00 for PGA6 and PGA8. Eight units have redness ratings ≥ 5.00 .

Most of the sediments in cores CGA and CGB are brown or yellowish brown. Redness ratings for core CGA range from 5.63 for CGA2 to 1.25 for CGA11 and CGA14; only CGA2 has a redness rating ≥ 5.00 . Redness ratings for core CGB range from 10.00 for CGB1 to 0.83 for CGB7 and CGB8; only three units (CGB1, CGB2 and CGB10) have redness ratings ≥ 5.00 . Sediments in core NR are strong brown to brown, with redness ratings ranging from 6.25 for NR20 to 0.75 for NR15; only three units (NR3, NR4 and NR20) have redness ratings ≥ 5.00 . In core CM, most sediments are greyish brown to brown, with redness ratings ranging from 25.00 for CM11 to 0.00 for CM4, CM12 and CM13. Five units have redness ratings ≥ 5.00 . In core TG, grey and brown colours predominate above TG14; below this the colours are mainly reddish to yellowish brown. Redness ratings range from 10.00 for TG2 to 0.00 for TG16, TG17, TG19, TG21 and TG22 and six units, all stratigraphically below TG16, have redness ratings ≥ 5.00 .

Table 6.15: Redness rating for Gordano Valley sediments

Unit	Redness rating	Unit	Redness rating	Unit	Redness rating	Unit	Redness rating	Unit	Redness rating
PG8	1.33	CGA14	1.25	NR26	0.00	CM13	0.00	TG8	3.75 to 1.67
PG7	5.00	CGA13	1.50 to 2.00	NR25	3.15 to 2.08	CM12	0.00	TG7	0.83 to 1.25
PG6	1.67	CGA12	4.17	NR24	4.17	CM11	25.00	TG6	5.00
PG5	0.00	CGA11	1.25	NR23	2.08	CM10	2.50	TG5	0.63
PG4	1.25	CGA10	3.33	NR22	4.17	CM9	2.50	TG4	4.38
PG3	0.00	CGA9	2.08	NR21	2.08	CM8	5.00	TG3	5.00
PG2	7.50	CGA8	3.13	NR20	6.25 to 3.13	CM7	1.00	TG2	10.00
PG1	0.00	CGA7	2.08	NR19	3.13	CM6	5.00	TG1	7.50
PGA17	5.00	CGA6	2.50	NR18	1.67 to 2.08	CM5	5.00		
PGA16	1.50	CGA5	1.56	NR17	3.13	CM4	0.00		
PGA15	5.00	CGA4	1.56	NR16	1.56	CM3	0.67		
PGA14	8.33	CGA3	2.50	NR15	0.75	CM2	2.08		
PGA13	5.00	CGA2	5.63	NR14	2.08	CM1	7.50		
PGA12	1.25	CGA1	2.50	NR13	1.67	TG22	0.00		
PGA11	6.25	CGB13	3.13	NR12	2.50	TG21	0.00		
PGA10	3.13	CGB12	1.25	NR11	0.83	TG20	1.33		
PGA9	3.13	CGB11	3.13	NR10	1.56	TG19	0.00		
PGA8	0.00	CGB10	7.50 to 2.08	NR9	1.56 to 4.17	TG18	3.75 to 2.00		
PGA7	4.17	CGB9	2.50	NR8	2.08	TG17	0.00		
PGA6	0.00	CGB8	0.83	NR7	2.08	TG16	0.00		
PGA5	6.25	CGB7	0.83	NR6	2.08	TG15	3.33		
PGA4	4.17	CGB6	1.56	NR5	2.50	TG14	3.33		
PGA3	5.00	CGB5	1.56	NR4	5.00	TG13	6.25 to 1.67		
PGA2	0.83	CGB4	3.75	NR3	5.00	TG12	1.67		
PGA1	11.25	CGB3	3.33	NR2	2.50	TG11	4.17		
		CGB2	6.67	NR1	2.08	TG10	1.00 to 3.75		
		CGB1	10.00			TG9	4.17		

6.9 Palaeontology

Some fossil remains are identified in a generalised way and these are described first. PG1 contains part of a burrow or root, approximately 10 mm in length and 1 mm wide (Figure 6.12), preserved by an infill of calcite. In PG3 a wood fragment is found; this is probably derived, and identification was not attempted.



Figure 6.12: Calcified burrow or root trace in PG1 (arrowed)

PGA11 mainly comprises a large, tapering, downward branching fossil root trace (Figure 6.2B), and its red colour is probably the result of preferential oxidation of sediment around the root trace (Tucker 2003). The sharp upper and lower boundaries recorded for PGA11 reflect the external boundaries of the root. A fossil root trace is also found in CGA11.

Fossil remains in core NR consist mainly of derived roots and reed stems. However, there are also *in situ* plant remains: vertically oriented organic material in NR26, the vertically oriented reed stem and roots in NR25, the vertically oriented reed stems in NR23, NR21, NR19 and NR17, and tangled fine roots in NR16 all indicate *in situ* growth; a vertically oriented *in situ* reed stem in NR25 had retained its green colour (Figure 6.13). Fossil remains in core CM consisted of vertically and sub-horizontally oriented plant stems, which have not been further identified.



Figure 6.13: Two views of *in situ*, vertically oriented green reed stem in NR25

Core TG however, contains two richly fossiliferous units, TG7 and TG8, which provide the most evidence for former environments. For this reason, these two units have been investigated in more detail than other units in which fossil evidence was noted. Fossil evidence is drawn from molluscs, ostracods, foraminifera, algae and coleoptera.

6.9.1 Molluscs

Results of mollusc analysis of TG7 and TG 8 are presented in Table 6.16. Many of the molluscs are undersized, either because they are juveniles or were environmentally stressed. The general condition of the mollusc shells in TG8 is good, with little evidence of iron staining or secondary calcite deposition. TG7 has comparatively fewer molluscs and most of those are poorly preserved, suggesting they may not be *in situ*. Both units have a freshwater assemblage; no terrestrial or intertidal molluscs were found in either unit.

Table 6.16: Molluscs recovered from TG7 and TG8. Numbers for *Sphaerium* and *Pisidium* refer to individual valves. *Lymnaea* spp. (undifferentiated) refers to *Lymnaea* apices with damaged or missing apertures that prevented accurate identification; indeterminate refers to bivalves too juvenile to identify

	TG8	TG7
Approximate weight of sample	110.66 g	23.99 g
<i>Radix balthica</i> (Linnaeus) (= <i>Lymnaea peregra</i> (Müller))	49	1
<i>Lymnaea</i> spp. (undifferentiated)	22	-
<i>Ancylus fluviatilis</i> (Müller)	12	3
<i>Valvata piscinalis</i> (Müller)	227	-
<i>Gyraulis laevis</i> (Alder)	19	2
<i>Pisidium obtusale</i> (Lamarck)	60	19
<i>Pisidium subtruncatum</i> (Malm)	7	7
<i>Pisidium nitidum</i> (Jenyns)	-	7
<i>Sphaerium corneum</i> (Sheppard)	18	4
Indeterminate	7	8
Total count	421	51

6.9.2 Ostracods

Results of ostracod analysis for TG7 and TG 8 are presented in Table 6.17. These are placed in three groups based on their salinity tolerance: Non-marine ostracods, some of which are able to tolerate low salinities; brackish estuarine ostracods, which inhabit tidal flats and creeks, and outer estuarine and marine ostracods, consisting of marine species which are able to penetrate outer estuaries. In addition, there are three groups of "Exotic" marine ostracods: cold "northern" marine species, warm "southern" marine species and shelf-living species which could have been brought into the Gordano Valley by tidal surges. Preservation of valves is generally good; there are some united valves in TG7 which suggests that at least some of the species are contemporary with the sediment. Some valves were broken, although breakage may have occurred during coring and sample processing. Thirty four ostracod species were identified and no one species was dominant in either unit. Despite a much lower volume of material from which the ostracods were extracted, TG7 has a much higher abundance (14/g) than TG8 (1/g), and a more diverse assemblage in terms of species (TG7 = 33; TG8 = 22). Figure 6.14 illustrates some of the ostracods collected from TG7 and TG8.



Figure 6.14: Some of the ostracods collected from TG7 and TG8. 1. *Limnocythere inopinata*; 2. *Hemicythere villosa*; 3. *Semicytherura sella*; 4. *Robertsonites tuberculatus*; 5. *Leptocythere psammophila*; 6. *Potamocypris zschokkei*; 7. *Aurila convexa*; 8. *Prionocypris zenkeri*

Only 20% of the ostracods found in TG8 are non-marine, whereas TG7 has 55% non-marine species, although some of the non-marine species are able to tolerate brackish conditions. Exotic species occur in both TG7 and TG8, forming a greater proportion in TG8. TG7 contains two valves (1%) which are indeterminate and forty five valves (13%) of either *Paradoxostoma* or *Sclerochilus* spp. which it was not possible to differentiate.

Table 6.17: Results of analysis for ostracods. Numbers refer to individual valves.

Nomenclature follows Meisch (2000)

NON-MARINE OSTRACODS	TG8	TG7
Approximate weight of sample	110.66 g	23.99 g
<i>Candona neglecta</i>	8	20
<i>Prionocypris zenkeri</i>	6	17
<i>Ilyocypris bradyi</i>	5	47
<i>Heterocypris salina</i>	1	58
<i>Potamocypris zschokkei</i>	1	11
<i>Limnocythere inopinata</i>	-	16
<i>Herpetocypris reptans</i>	-	10
<i>Cypridopsis vidua</i>	-	8
<i>Cycloocypris ovum</i> (RV>LV)	-	5
Indeterminate	-	2
<i>Pseudocandona</i> sp.	-	1
Total count	21	195
BRACKISH ESTUARINE OSTRACODS	TG8	TG7
<i>Leptocythere psammophila</i>	10	42
<i>Leptocythere lacertosa</i>	-	2
<i>Cyprideis torosa</i>	-	1
Total count	10	45
OUTER ESTUARINE & MARINE OSTRACODS	TG8	TG7
<i>Hemicythere villosa</i>	14	11
<i>Hirschmannia viridis</i>	13	9
<i>Hemicytherura cellulosa</i>	6	1
<i>Palmoconcha laevata</i>	5	5
<i>Leptocythere tenera</i>	5	9
<i>Semicytherura sella</i>	2	2
<i>Semicytherura</i> spp.	2	2
<i>Cytheropteron nodosum</i>	1	1
<i>Semicytherura nigrescens</i>	1	-
<i>Semicytherura simplex</i>	1	-
<i>Paradoxostoma/Sclerochilus</i> spp.	1	45
<i>Eucythere declivis</i>	-	1
<i>Pontocypris mytiloides</i>	-	1
<i>Bythocythere</i> sp.	-	1
Total count	51	88

Table 6.17: (continued): Results of analysis for ostracods

"EXOTIC" MARINE OSTRACODS	TG8	TG7
<i>Hemicytherura clathrata</i>	12	10
<i>Finmarchinella angulata</i>	3	4
<i>Finmarchinella finmarchica</i>	3	2
<i>Robertsonites tuberculatus</i>	2	1
<i>Aurila convexa</i>	4	6
<i>Xestoleberis labiata</i>	-	1
<i>Neonesidea globosa</i>	-	2
Total count	24	26
TOTAL	106	354

6.9.3 Foraminifera

Results of foraminiferal analysis of TG7 and TG 8 are presented in Table 6.18. The foraminifera belong to two groups: brackish water estuarine taxa and marine shelf taxa. Preservation of valves is generally good, although many of the *Elphidium* were identified as *williamsoni* due to lack of bosses or keels and the size of their retral processes. There were also some more opaque specimens which are likely to be interglacial or glacial marine and some very small specimens which could be juveniles that were preferentially transported, or they could be very small glacial species.

Sixteen foraminifera species were identified and both units are dominated by *Elphidium williamsoni*, *Cibicides lobatulus* and *Haynesina germanica*. The two units have similarly diverse assemblages, but have different species composition.

Table 6.18: Results of analysis for foraminifera.

Uncertain identification is marked thus: ?

	TG8	TG7
<i>Elphidium williamsoni</i>	43	81
<i>Cibicides lobatulus</i>	52+1?	31+5?
<i>Brizalina pseudopunctata</i>	2	-
<i>Elphidium incertum?</i>	3	-
<i>Haynesina germanica</i>	30	25+3?
<i>Lagena spp.</i>	3	5
<i>Elphidium macellum</i>	1	-
<i>Ammonia becarrii</i>	1	-
<i>Asterigerinata mamilla</i>	6	11+1?
<i>Haynesina depressulus</i>	2	1?
<i>Lagena sulcata</i>	3	8
<i>Globergerina spp.</i>	3	-
<i>Patellina corrugata</i>	-	12
<i>Oolina spp</i>	-	3
<i>Spirillina vivipara</i>	-	1
<i>Elphidium crispum</i>	-	1
Unidentified	8	-
Total	157+1?	178+10?

6.9.4 Algae

Both TG7 and TG8 contained fragments of the freshwater alga *Chara*; examples are illustrated in Figure 6.15. The fragments were more abundant in TG7 than in TG8, and included oospores with the characteristic spiral ridges of charophytes and vegetative structures with cross sections of stem showing a cortex around a large central syphon, indicative of the genus *Chara*, although limited characteristics prevented identification to species level.

The *Chara* fragments recovered from TG7 were in a good state of preservation. Most of the oospores were intact, although some ridges were abraded; three were broken, one revealing a dark core, and eight others were dark coloured rather than white. Despite calcite encrustation, the distinctive torque of the stem was visible on some stems, and some stems display evidence of branchlets. The *Chara* fragments recovered from TG8 were

generally in a poor state of preservation. Only two oospores were intact; a third one was broken.

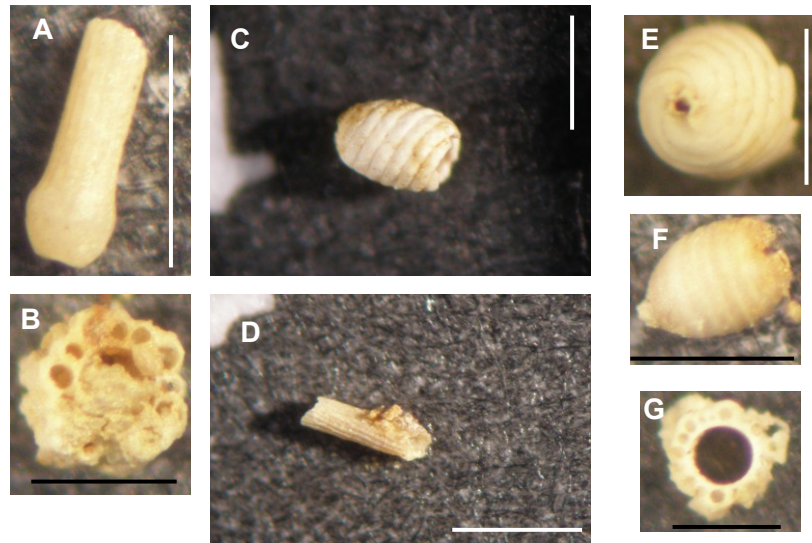


Figure 6.15: Charophyte fragments recovered from TG7 and TG8. A & D. Stems. C, E & F. Oospores. B & G. Cross-section of stems showing the central syphon surrounded by a cortex. Bars for scale: A: 700 μm ; B: 500 μm ; C: 750 μm ; D: 600 μm ; E: 500 μm ; F: 550 μm ; G: 400 μm

6.9.5 Coleoptera

The remains of a beetle of the *Staphylinidae* family, probably part of the underbody, were found in TG7. However, disarticulation has prevented full identification.

6.10 Geochronology

Two bulk sediment samples, one from the top of CGA6, and one from the top of NR15, units identified from the stratigraphy as showing indications of pedogenesis (Figures 6.3A and C and 6.6 A and C), were sent to Beta Analytic for AMS radiocarbon dating of soil organic matter. The submitted samples underwent acid wash pre-treatment and dates were calibrated using INTCAL04 (Reimer *et al.* 2004). A 2 Sigma calibrated result (95% probability) of 22280 to 21810 Cal BP; (1 Sigma calibrated result (68% probability) of 22200 to 22000 Cal BP; conventional radiocarbon age: 18480 \pm 120 BP) was returned for CGA6. A 2 Sigma calibrated result (95% probability) of 13430 to 13190 Cal BP; (1 Sigma

calibrated result (68% probability) of 13380 to 13230 Cal BP; conventional radiocarbon age of 11450 ± 60 BP) was returned for NR15.

A sample of freshwater mollusc shells from TG8 was also sent to Beta Analytic for AMS radiocarbon dating. The submitted sample underwent acid-etch pre-treatment to eliminate secondary carbonate components. A date of 45460 ± 790 BP was returned. This date is very close to the limit of the technology, and Pigati *et al.* (2007) and Briant and Bateman (2009) have recommended that conventionally pre-treated radiocarbon ages older than 35^{14}C ka BP should be treated with caution.

Five *Valvata piscinalis* shells from TG8 were also analysed for the degradation of intra-crystalline proteins using the AAR technique developed for geochronology (Penkman *et al.* 2007, Penkman *et al.* 2008). The samples were prepared using the procedures outlined in Penkman *et al.* (2008) to isolate the intra-crystalline protein by bleaching. Two sub-samples were taken from each shell: one for analysis for free amino acids (FAA) and one for the total hydrolysable amino acids (THAA). Samples were analysed in duplicate by RPC. The extent of racemization in five amino acids (D/L of aspartic acid/asparagine (Asx), glutamic acid/glutamine (Glx), serine (Ser) alanine (Ala) and valine (Val), along with the ratio of concentration of Ser to Ala ([Ser]/[Ala]), are shown in Table 6.19. One sample (NEaar 6170bH*) was not analysed due to difficulties during preparation.

Figure 6.16 shows D/L values of Asx, Glx and Ala for the FAA and THAA fractions of the TG8 shells compared with shells from other sites in southern England with independent geochronology. The variability of AAR results from the TG8 dataset is quite high, resulting in less clear separation when compared to the other sites. The D/L Asx data show values similar to samples of MIS 5e age, but with THAA values indistinguishable from MIS 7. The Glx D/L values show values consistent with an MIS 5e age, although some overlap with the lower values of the MIS 7 range. The results for Ala show that the extent of protein breakdown in the samples from TG8 is similar to that of the youngest MIS 7 samples. The data obtained from these amino acids are consistent with an age of MIS 5e or MIS 7.

The data from serine and valine are less useful for samples of this age; serine racemizes rapidly, so samples of this age are nearing equilibrium. Valine has extremely low rates of racemization, and as the concentration of Val is quite low, the difficulty of measuring the D/L results in higher variability. On the basis of the relative D/L values and

concentrations the results obtained indicate a late MIS 7 or possibly early MIS 5e age (K.E.H. Penkman, 2010, Pers. comm.).

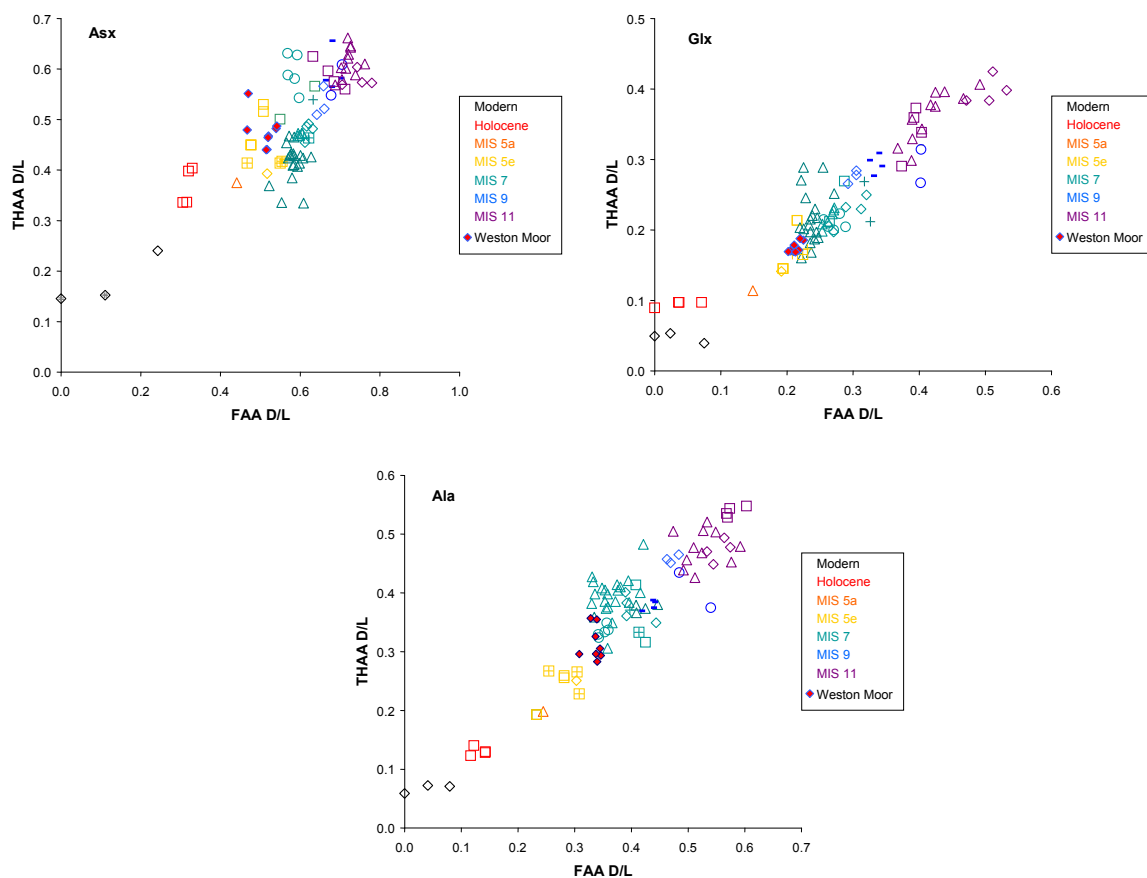


Figure 6.16: D/L values of Asx, Glx and Ala for the FAA and THAA fractions of the bleached *Valvata piscinalis* shells from TG8 (labelled ‘Weston Moor’) compared with shells from other sites from southern England with independent geochronology

Six samples for OSL dating were taken from a sediment core (TG-OSL) extracted from Weston Moor, (UK grid reference ST 44451234 73573798), located approximately 1 m from the location of the core TG. The core comprises a sequence of 2.44 m of sands and gravels overlain by 1.22 m of marl which is in turn overlain by 1.13 m of muds and 2.99 m peat. The stratigraphy of core TG-OSL, and the units from which samples were taken for dating, is shown in Figure 6.17. Two samples were taken from each 1 m section of core, and were assigned laboratory numbers x3780-x3785; X3785 and x3781 were taken from gravel units and x3780, x3782, x3783, and x3784 were taken from fine sand. Sample preparation and analysis was carried out using the protocols described in section 4.11.3. The results are summarised in Table 6.20.

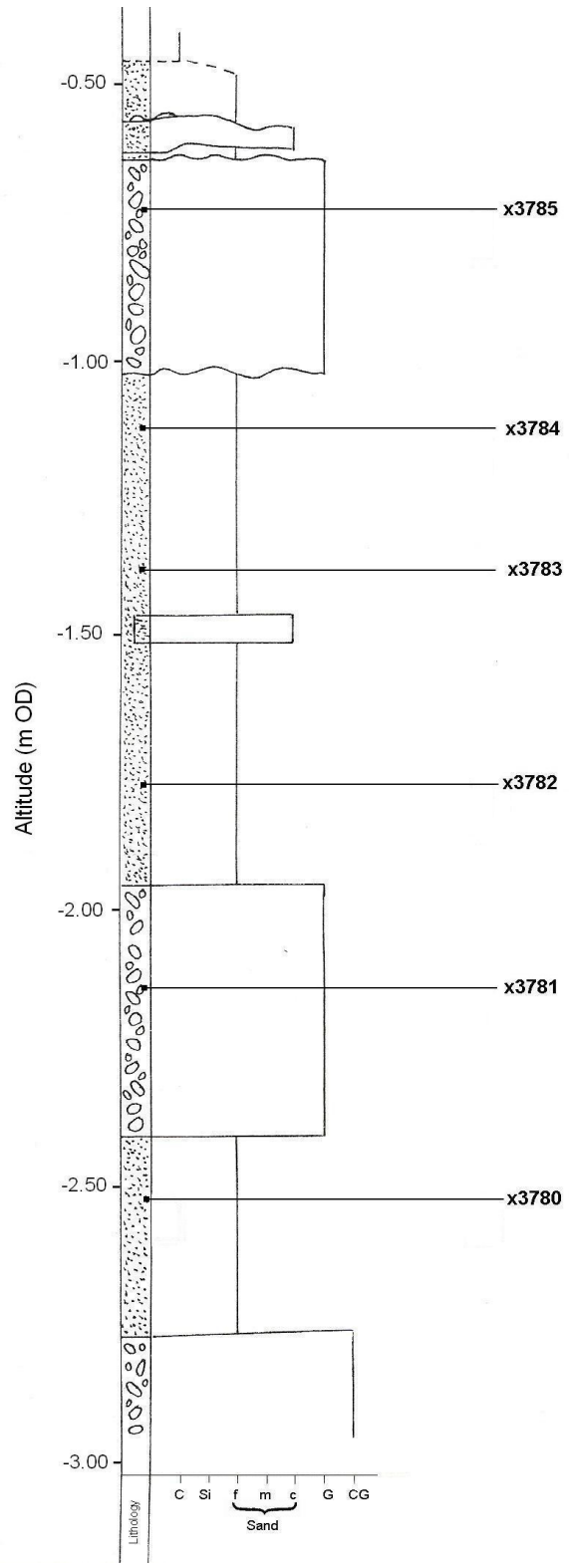


Figure 6.17: Stratigraphy of core TG-OSL showing locations of samples taken for OSL dating

Table 6.19: Amino acid data from *Valvata piscinalis* shells from TG8. Each sample was bleached (b). The FAA fraction is signified by 'F' and the THAA fraction is signified by 'H*'. NEaar is North East amino acid racemization, and is a unique identifier for the sample

NEaar	Sample	Asx D/L	Glx D/L	Ser D/L	Ala D/L	Val D/L	[Ser]/[Ala]
6168bF	ABVp1bF	0.470 ± 0.000	0.210 ± 0.000	0.863 ± 0.029	0.340 ± 0.007	0.137 ± 0.004	0.280 ± 0.040
6168bH*	ABVp1bH*	0.515 ± 0.035	0.170 ± 0.000	0.670 ± 0.010	0.310 ± 0.020	0.165 ± 0.005	0.325 ± 0.035
6169bF	ABVp2bF	0.540 ± 0.000	0.223 ± 0.004	0.817 ± 0.009	0.320 ± 0.007	0.143 ± 0.011	0.367 ± 0.031
6169b H*	ABVp2b H*	0.485 ± 0.005	0.190 ± 0.000	0.735 ± 0.015	0.330 ± 0.030	0.135 ± 0.015	0.275 ± 0.015
6170bF	ABVp3bF	0.520 ± 0.010	0.215 ± 0.005	0.630 ± 0.250	0.335 ± 0.015	0.135 ± 0.005	0.245 ± 0.095
6171bF	ABVp4bF	0.515 ± 0.005	0.205 ± 0.005	0.745 ± 0.065	0.340 ± 0.000	0.165 ± 0.015	0.280 ± 0.100
6171bH*	ABVp4bH*	0.440 ± 0.000	0.175 ± 0.005	0.235 ± 0.235	0.315 ± 0.035	0.245 ± 0.015	0.235 ± 0.165
6172bF	ABVp5bF	0.520 ± 0.000	0.215 ± 0.005	0.885 ± 0.005	0.340 ± 0.000	0.170 ± 0.010	0.290 ± 0.060
6172bH*	ABVp5bH*	0.465 ± 0.005	0.170 ± 0.000	0.685 ± 0.015	0.305 ± 0.005	0.170 ± 0.010	0.230 ± 0.140

Table 6.20: Summary of optically stimulated luminescence (OSL) dating results for TG-OSL

Lab. code	Sample description	Depth below surface(m)	Altitude (m OD)	Palaeodose (Gy)	Dose rate (Gy/ka)	Age estimate (ka)
X3785	Gravel matrix	5.80	-0.73	86.84 ± 14.47	0.95 ± 0.06	91 ± 16
X3784	Fine sand	6.22	-1.15	96.15 ± 20.41	1.54 ± 0.10	62 ± 14
X3783	Fine sand	6.39	-1.32	135.76 ± 14.75	1.50 ± 0.10	91 ± 12
X3782	Fine sand	6.78	-1.71	149.42 ± 11.79	1.68 ± 0.12	89 ± 9
X3781	Gravel matrix	7.23	-2.16	73.58 ± 2.25	0.79 ± 0.05	93 ± 7
X3780	Fine sand	7.63	-2.56	158.62 ± 21.64	1.75 ± 0.12	91 ± 14

Dose rate calculations are based on the concentration of radioactive elements (potassium, thorium and uranium) derived from elemental analysis by ICP-MS/AES using a fusion sample preparation technique and are based on Aitken (1985). These incorporated beta attenuation factors (Mejdahl 1979), dose rate conversion factors (Adamiec and Aitken 1998) and an absorption coefficient for the water content (Zimmerman 1971). The OSL age estimates include an additional 2% systematic error to account for uncertainties in source calibration. The contribution of cosmic radiation to the total dose rate was calculated as a function of latitude, altitude, burial depth and average over-burden density based on data by Prescott and Hutton (1994). There appears to be no systematic increase in OSL with depth, suggesting that deposition was relatively rapid.

The results for the stratigraphic analysis and sedimentology of the Gordano Valley Pleistocene minerogenic sediments presented above have demonstrated that a number of discrete depositional events have occurred in the Gordano Valley. In the next chapter these results are used to characterise and interpret the sediments in terms of their depositional and post-depositional environments.